Supplement of Atmos. Chem. Phys., 17, 9979–10000, 2017
https://doi.org/10.5194/acp-17-9979-2017-supplement

Atmospheric Chemistry and Physics
Open Access

Supplement of

Seasonal variations in high time-resolved chemical compositions, sources, and evolution of atmospheric submicron aerosols in the megacity Beijing

Wei Hu et al.

Correspondence to: Min Hu (minhu@pku.edu.cn)

S1 Sampling site and measurements

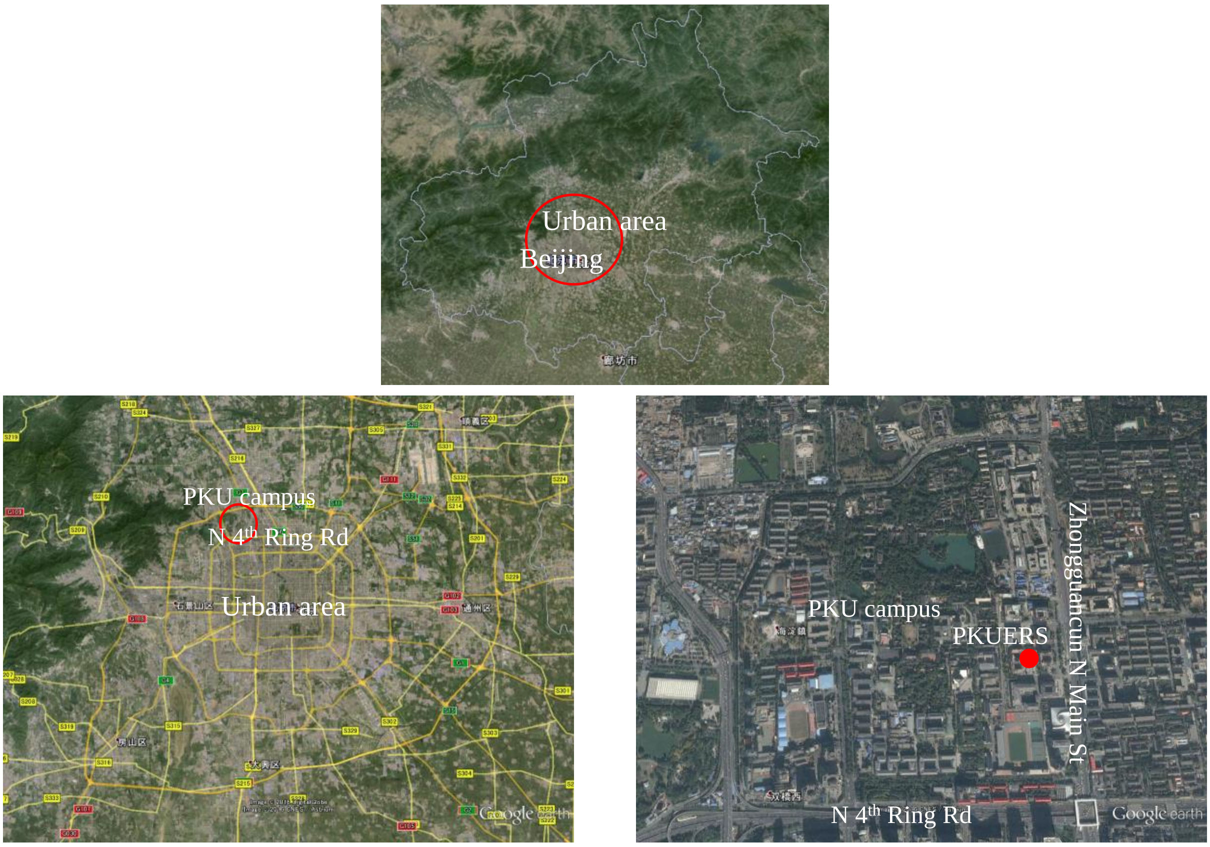

Figure S1. Location of observation site (PKUERS) and topographic map of Beijing.

Table S1 Measurement instrumentation for the campaigns.

Instrument	Parameters	Size	Time resolution	Manufacturer
HR-ToF-AMS	Mass concentrations size distributions of submicron non-refractory species	60~600 nm	4 min	Aerodyne Research Inc., USA
MAAP/Aethalometer	Particle absorption coefficient (BC)	2.5 µm	5 min	Thermo/Magee Scientific Co., USA
Semi-continuous EC/OC analyzer	Mass concentrations of OC and EC	2.5 µm	1 h	Sunset Lab Inc., USA
SMPS	Number concentrations of atmospheric particles	15~600 nm	5 min	TSI Inc., USA
TEOM 1400a, b	$PM_{2.5}$	2.5 µm	1 min	Thermo Scientific Co., USA
PTR-MS	Multiple volatile organic compounds (VOCs)		30 s	Ionicon Analytik, Austria
Gaseous pollutants	SO_2, NO_x, NO_y, CO, O_3		1 min	Ecotech Inc., USA
Meteorology	Wind speed and direction, temperature, relative humidity, atmospheric pressure		1 min	Met One Instruments Inc., USA

S2 Parameters of the AMS instrument

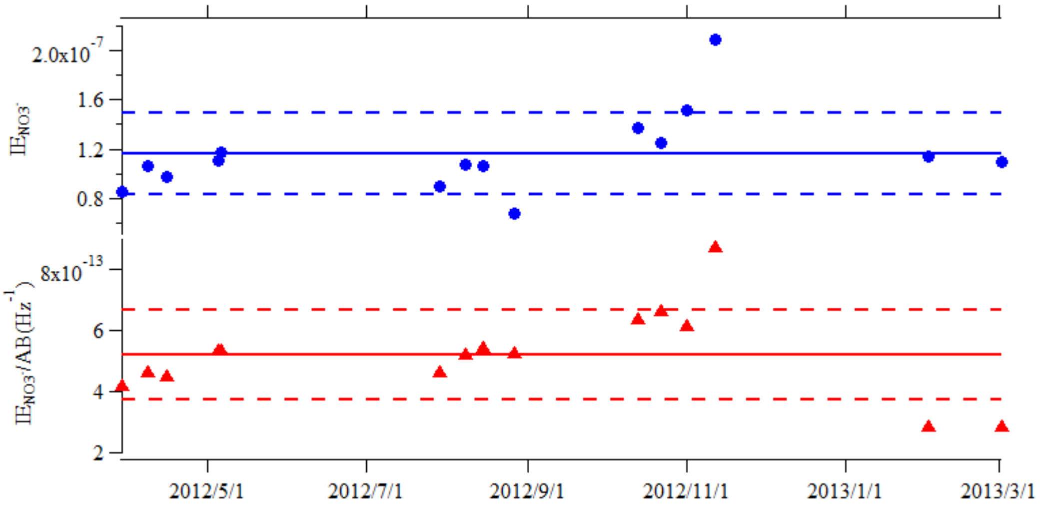

Figure S2. Ion efficiency (IE) and IE/air beam (AB) of the AMS in this study. The dashed line is the standard deviation of the average IE/AB (solid line).

Table S2 Detection limits (V-mode) of main components of aerosol detected by the AMS in this study. Units are μg m^{-3}. Detection limit of each species was determined by three times the standard deviations of detected signal of this species under particle-free condition.

Campaigns	OA	NO_3^-	SO_4^{2-}	NH_4^+	Cl^-
Spring	0.102	0.026	0.026	0.076	0.051
Summer	0.202	0.045	0.073	0.094	0.053
Autumn	0.337	0.019	0.017	0.068	0.025
Winter	0.072	0.016	0.022	0.043	0.014

S3 Comparison of results between AMS and other instruments, and ammonium balances

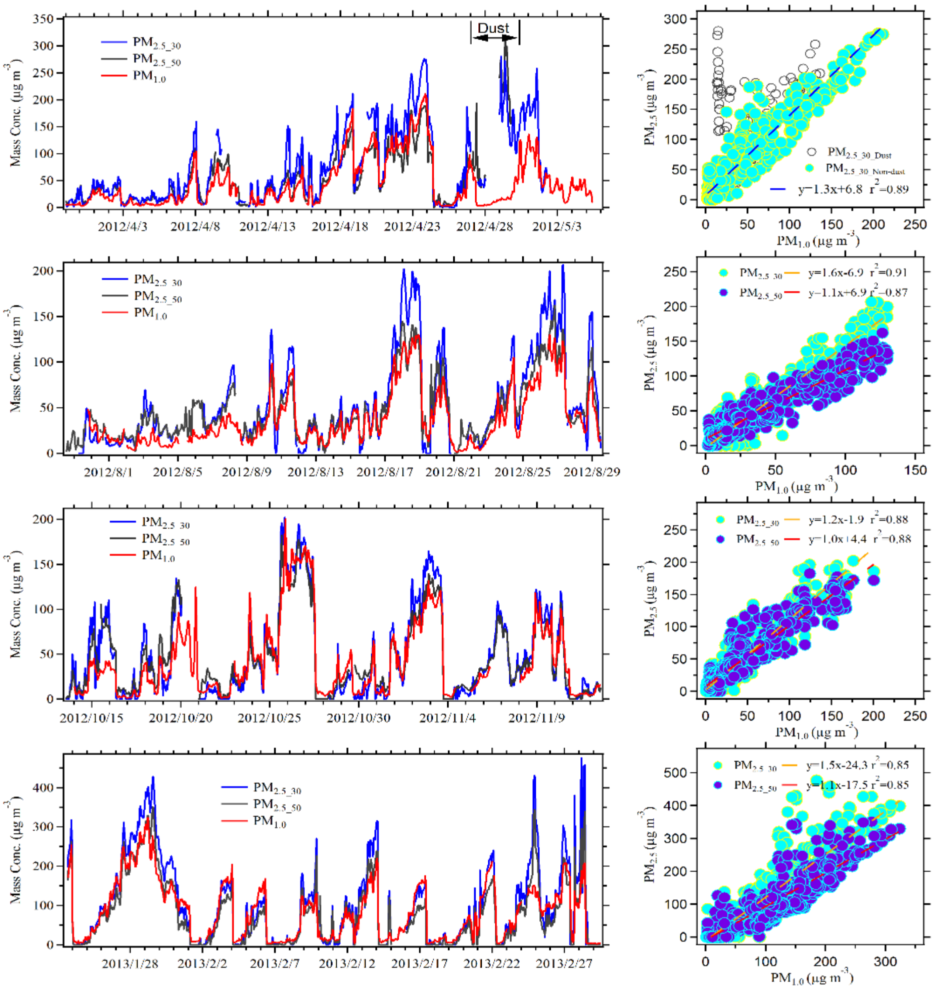

Figure S3. Time series and scatter plot of aerosol mass concentrations detected by the AMS plus BC vs. TEOM during seasonal observations. The size cut off for BC is $PM_{2.5}$. The size cut of TEOM is $PM_{2.5}$, which should be the main reason that lower concentration in AMS+BC observed. $PM_{2.5\_30}$ and $PM_{2.5\_50}$ mean the concentrations of fine particles with dehumidification at 30°C and 50°C, respectively.

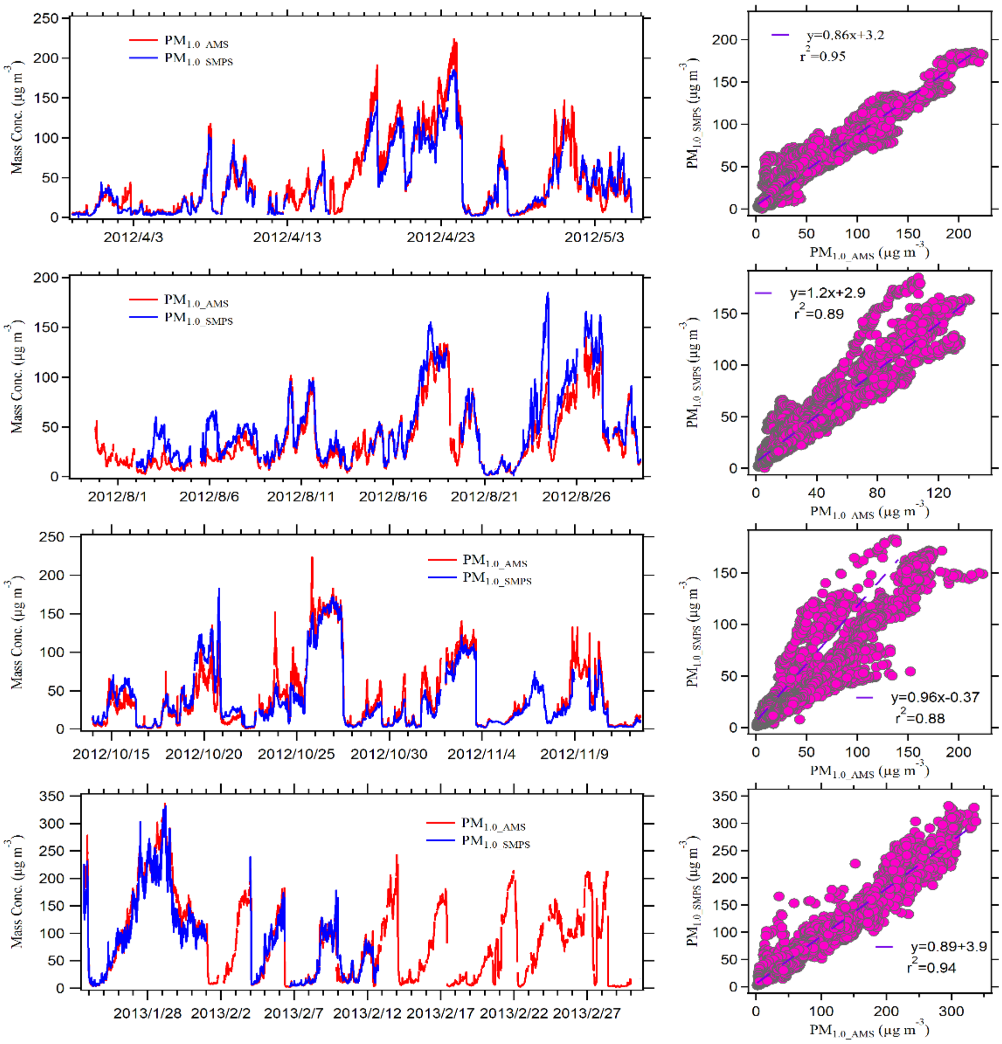

Figure S4. Time series and scatter plots of aerosol mass concentrations detected by the AMS plus BC vs. SMPS during seasonal observations. The aerosol density based on chemical composition of aerosols was used to convert SMPS volume concentrations to be mass concentrations (Middlebrook et al., 2012).

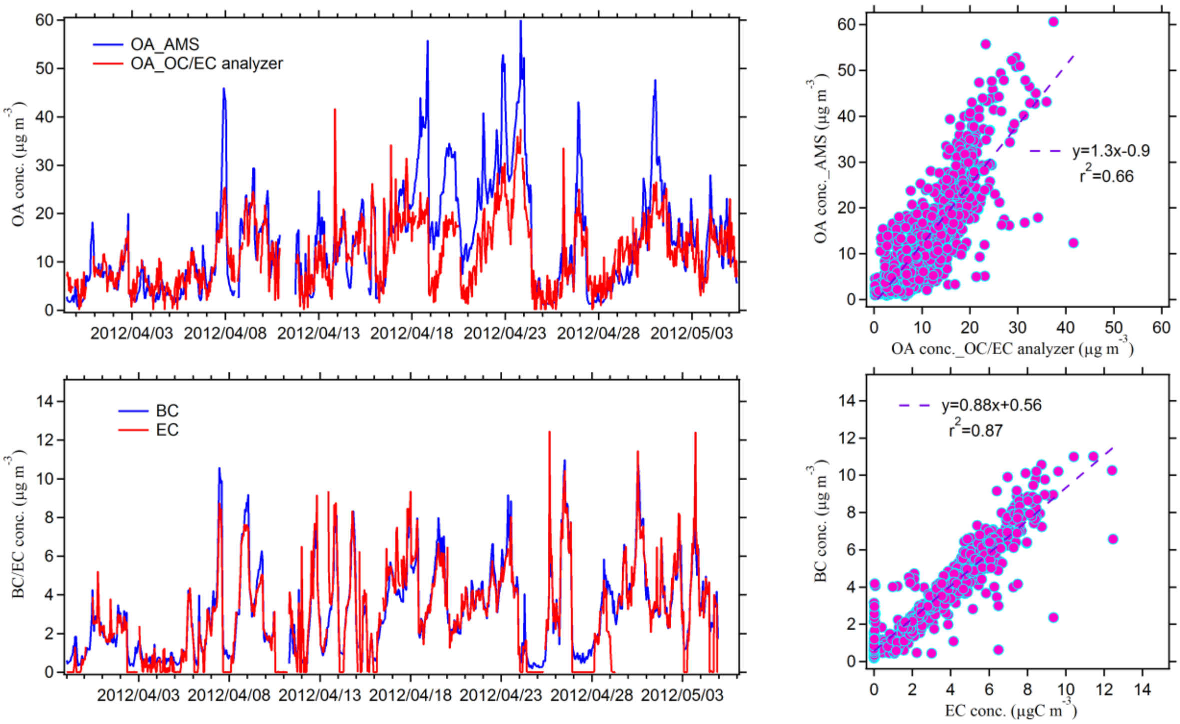

Figure S5. Time series and scatter plots of OA detected by the AMS vs. OA converted from OC measured by a semi-continuous OC/EC analyzer ($PM_{2.5}$ cutoff) using the OA/OC ratios measured by AMS, and BC vs. EC during the spring observation.

OA concentrations measured by the AMS showed tight correlation with the OC concentrations measured by a Sunset OC/EC Analyzer (r^2 =0.61). The linear regression slope of 2.4 is comparable to or within the range (2.0–2.7) of the previous results (Sun et al., 2011; Hu et al., 2013; Lan et al., 2011; Weimer et al., 2006), but is higher than the average OA/OC ratio of 1.81 determined via elemental analysis of the AMS. When the OM were at high concentration levels, the OA converted from OC measured by the OC/EC analyzer, using the OA/OC ratios measured by the AMS, deviated more from the OA time-series trends, consistent with the result of Lan et al. (2011). Possible reasons for this discrepancy include: (1) evaporative losses of semi-volatile organic species due to striking the balance of gas-particle partition after passing the activated-carbon denuder (Grover et al., 2008), and during the carbon analysis (Sun et al., 2011); (2) “over-calibration” of the OC data using the blank filter values (Bae et al., 2006).

S4 Variations of meteorological parameters and main compositions in PM_1

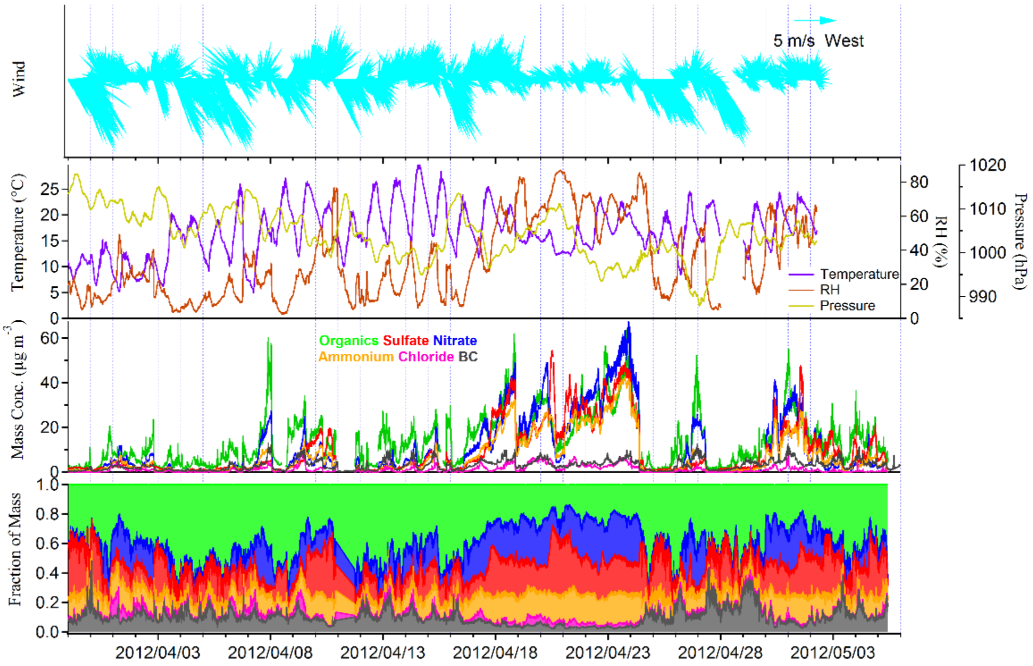

Figure S6. Time series of meteorological parameters (wind speed and direction, temperature, relative humidity (RH), and atmospheric pressure), and concentrations and fractions of main chemical compositions in submicron aerosols during the spring observation.

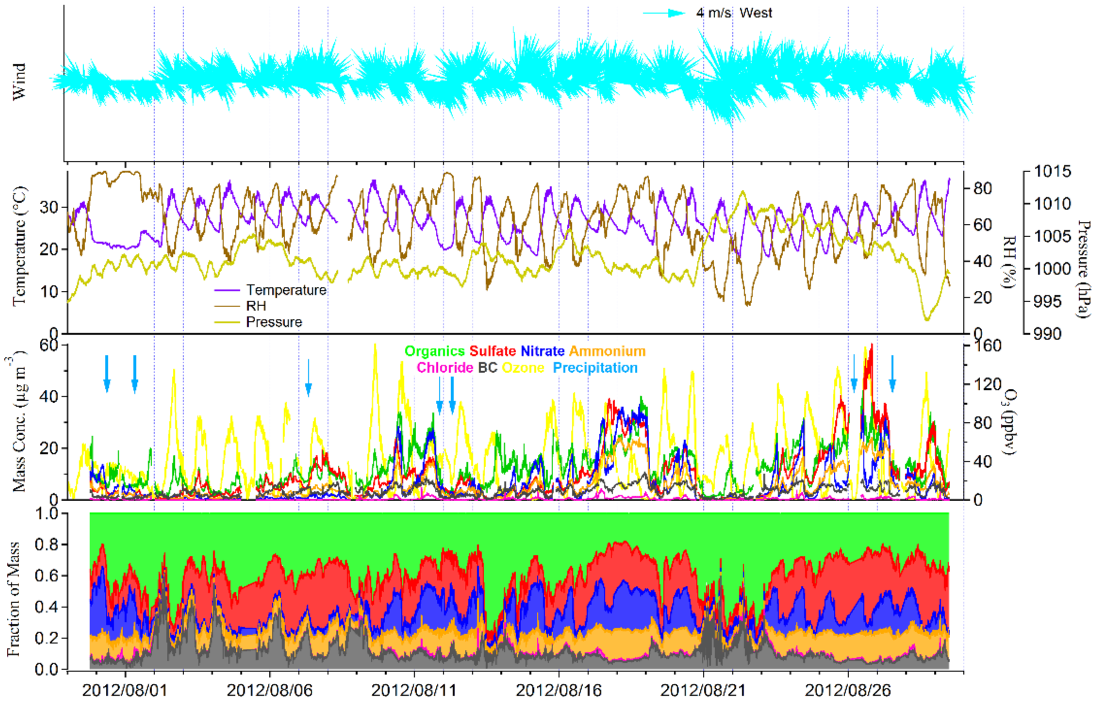

Figure S7. Time series of meteorological parameters (wind speed and direction, temperature, RH, and atmospheric pressure), and concentrations and fractions of main chemical compositions in submicron aerosols during the summer observation.

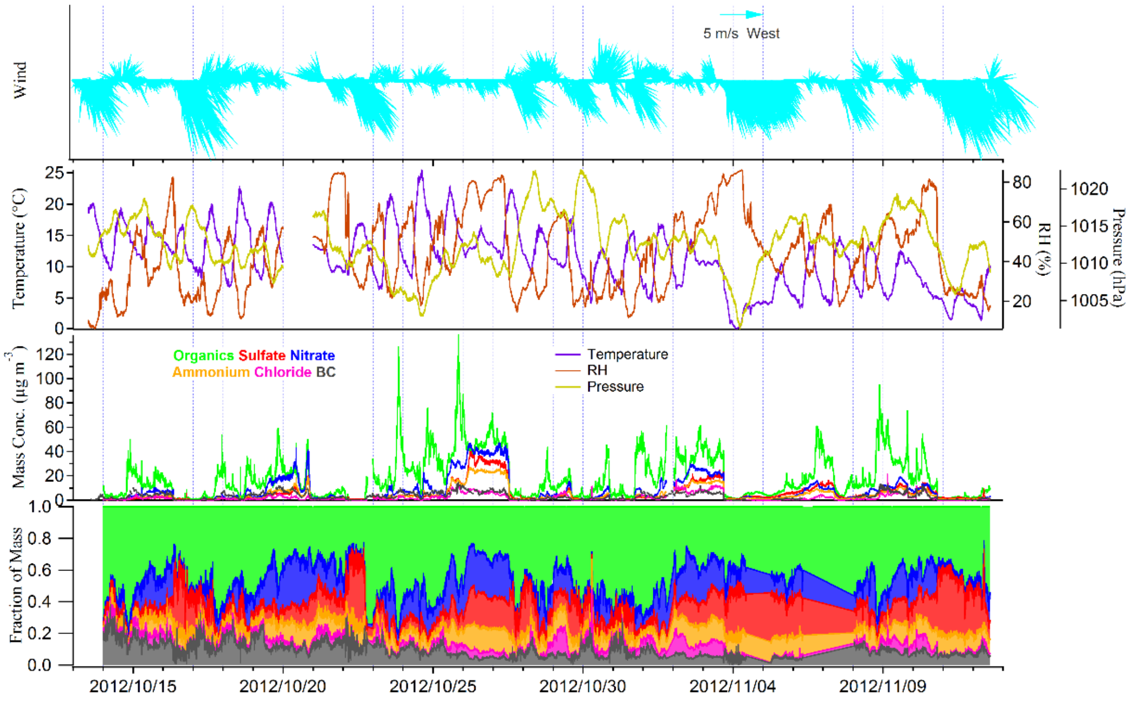

Figure S8. Time series of meteorological parameters (wind speed and direction, temperature, RH, and atmospheric pressure), and concentrations and fractions of main chemical compositions in submicron aerosols during the autumn observation.

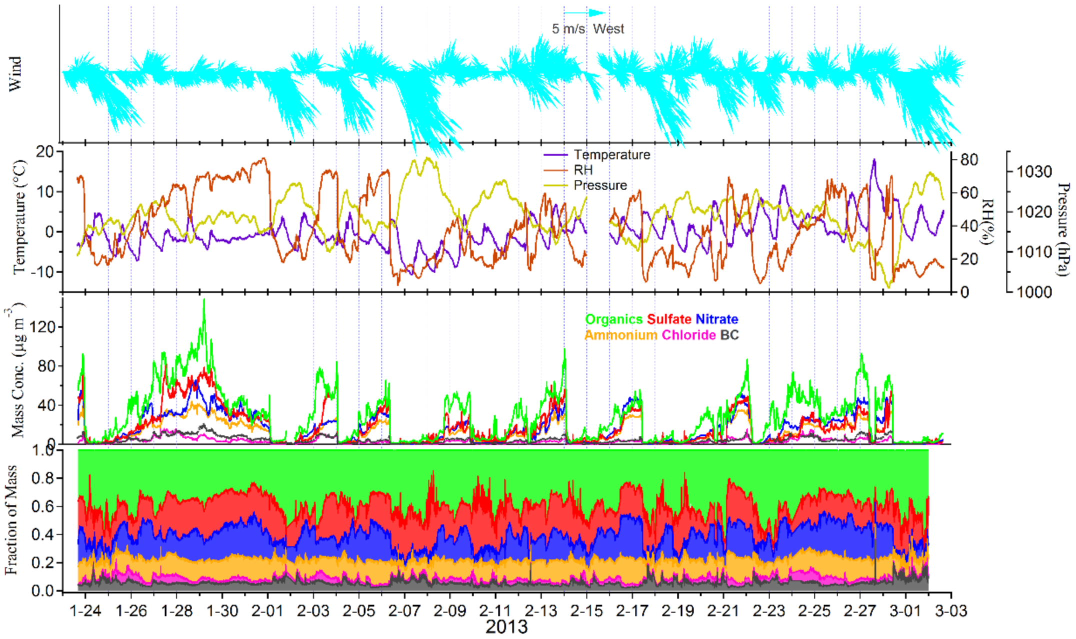

Figure S9. Time series of meteorological parameters (wind speed and direction, temperature, RH, and atmospheric pressure), and concentrations and fractions of main chemical compositions in submicron aerosols during the winter observation.

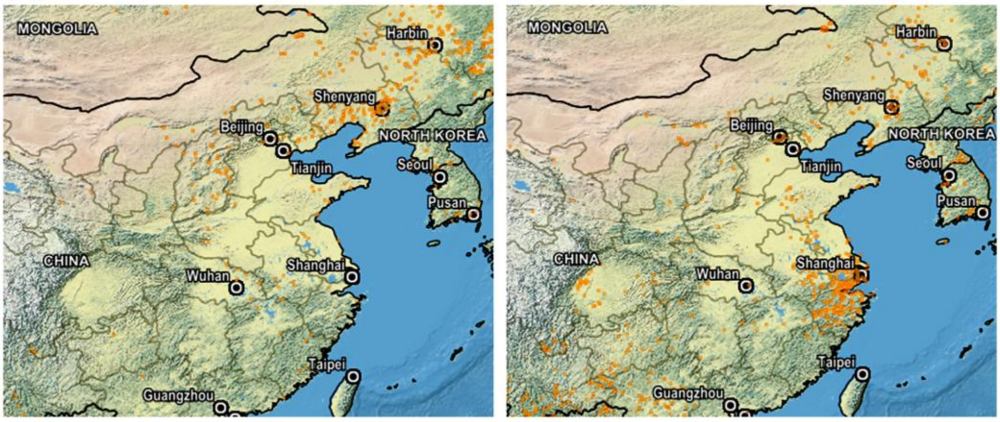
(a) 7-8 Apr. 2012 (UTC)

(b) 26-28 Apr. 2012 (UTC)

Figure S10. Fire points observed by satellites (https://firms.modaps.eosdis.nasa.gov/firemap) in Beijing and surrounding areas during 7–8 (a) and 26–28 (b) Apr. 2012.

(a) 18-20 Oct. 2012 (UTC)

(b) 23-27 Oct. 2012 (UTC)

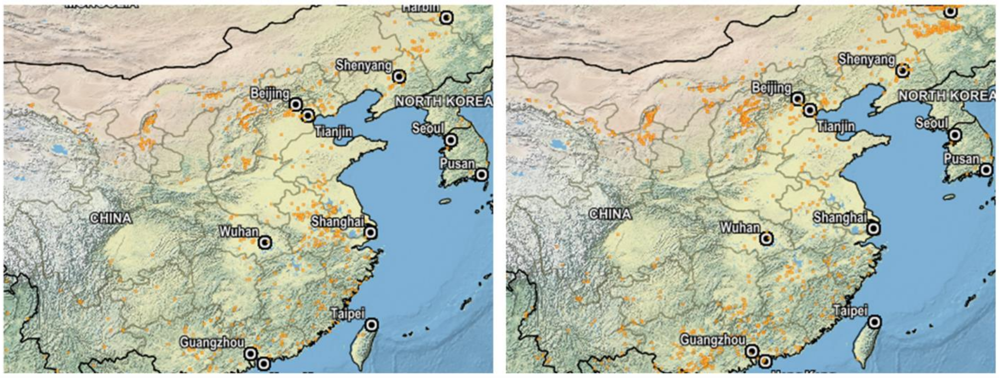

(c) 31 Oct.-3 Nov. 2012 (UTC)

(d) 6-11 Nov. 2012 (UTC)

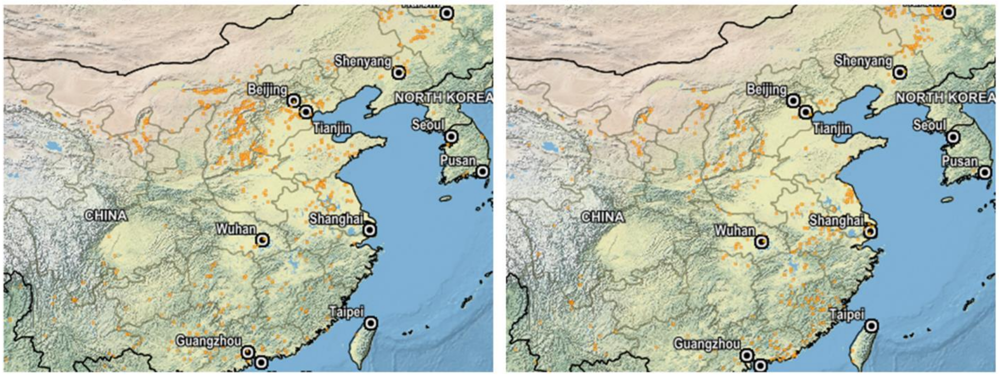

Figure S11. Fire points observed by satellites (https://firms.modaps.eosdis.nasa.gov/firemap) in Beijing and surrounding areas during the autumn observation.

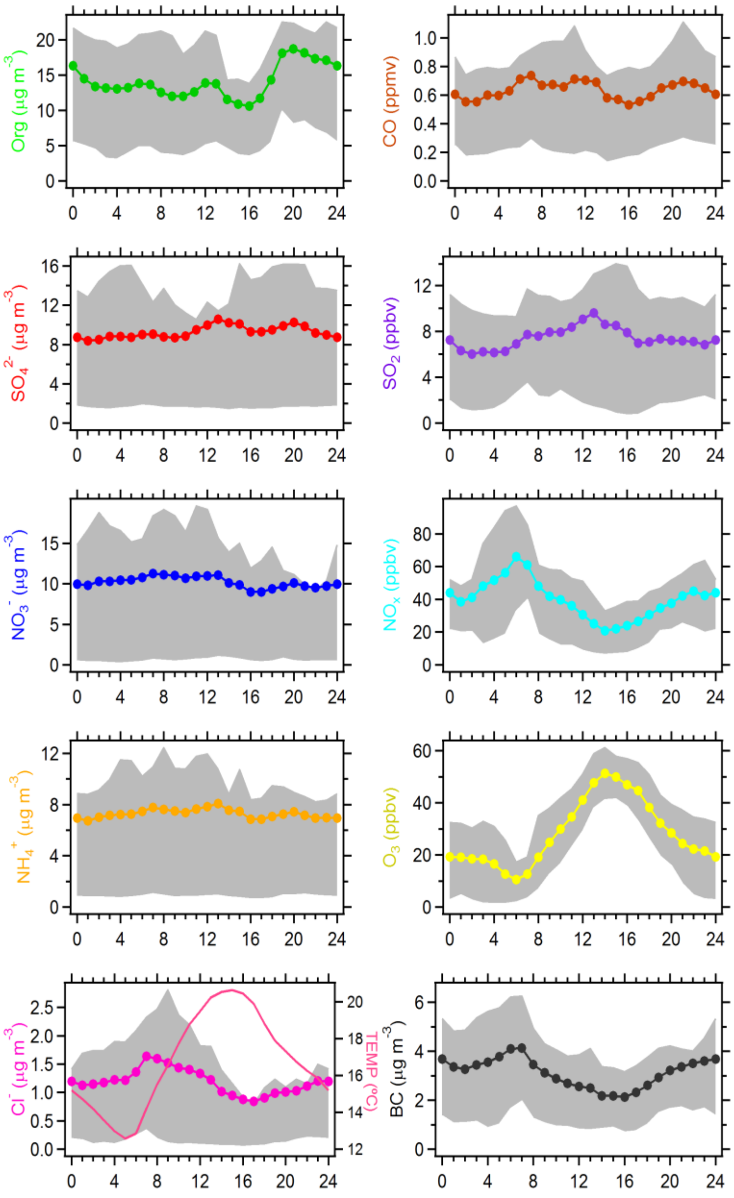

Figure S12. Diurnal patterns of chemical species of submicron particles and gaseous pollutants during the spring observation. The shaded area is between the 25% and 75% quantiles.

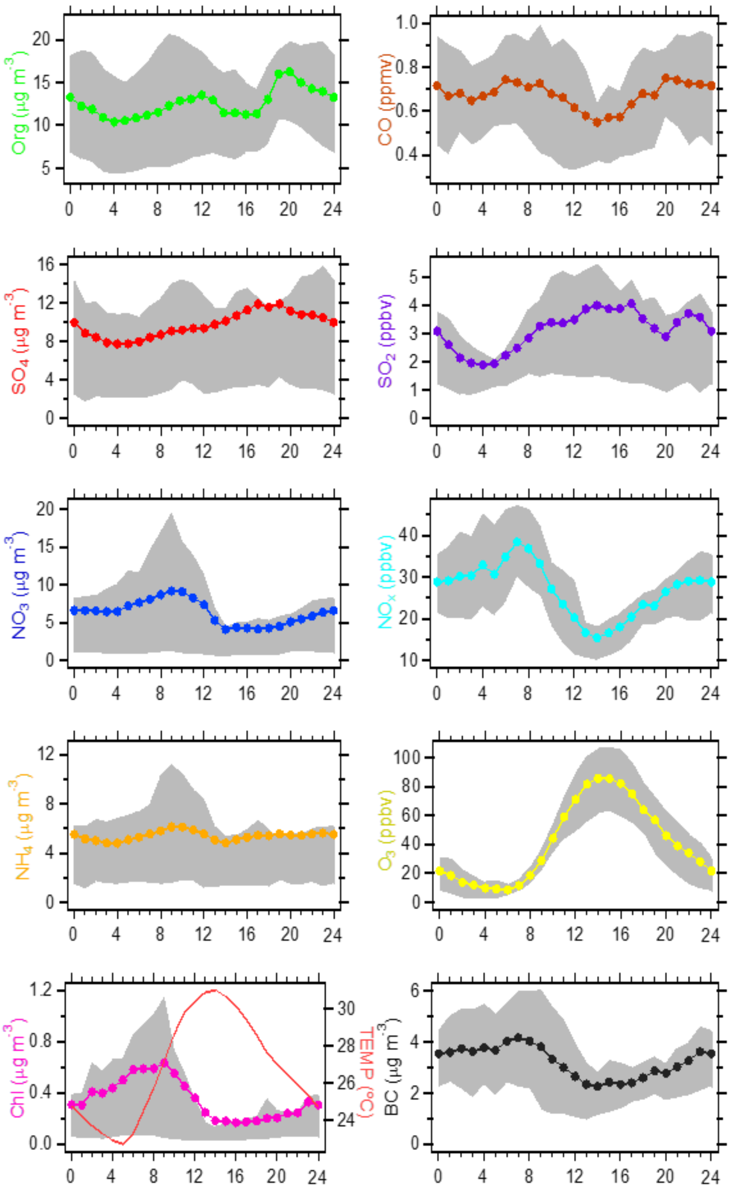

Figure S13. Diurnal patterns of chemical species of submicron particles and gaseous pollutants during the summer observation. The shaded area is between the 25% and 75% quantiles.

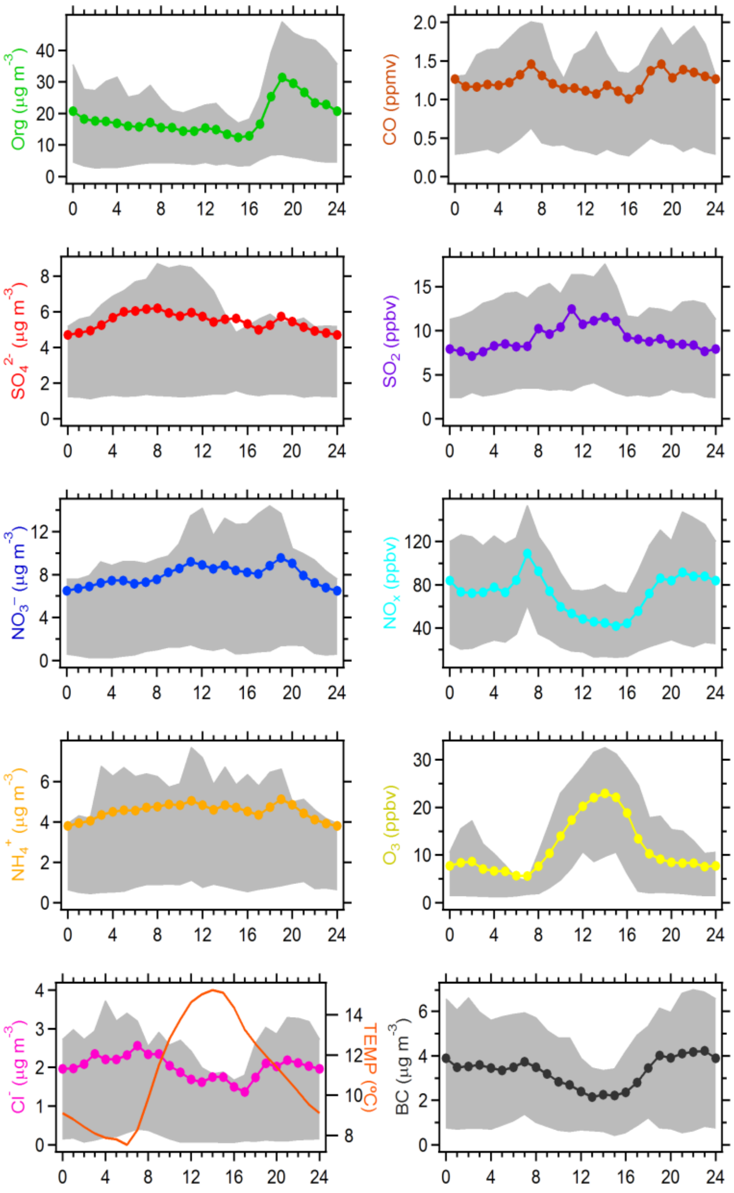

Figure S14. Diurnal patterns of chemical species of submicron particles and gaseous pollutants during the autumn observation. The shaded area is between the 25% and 75% quantiles.

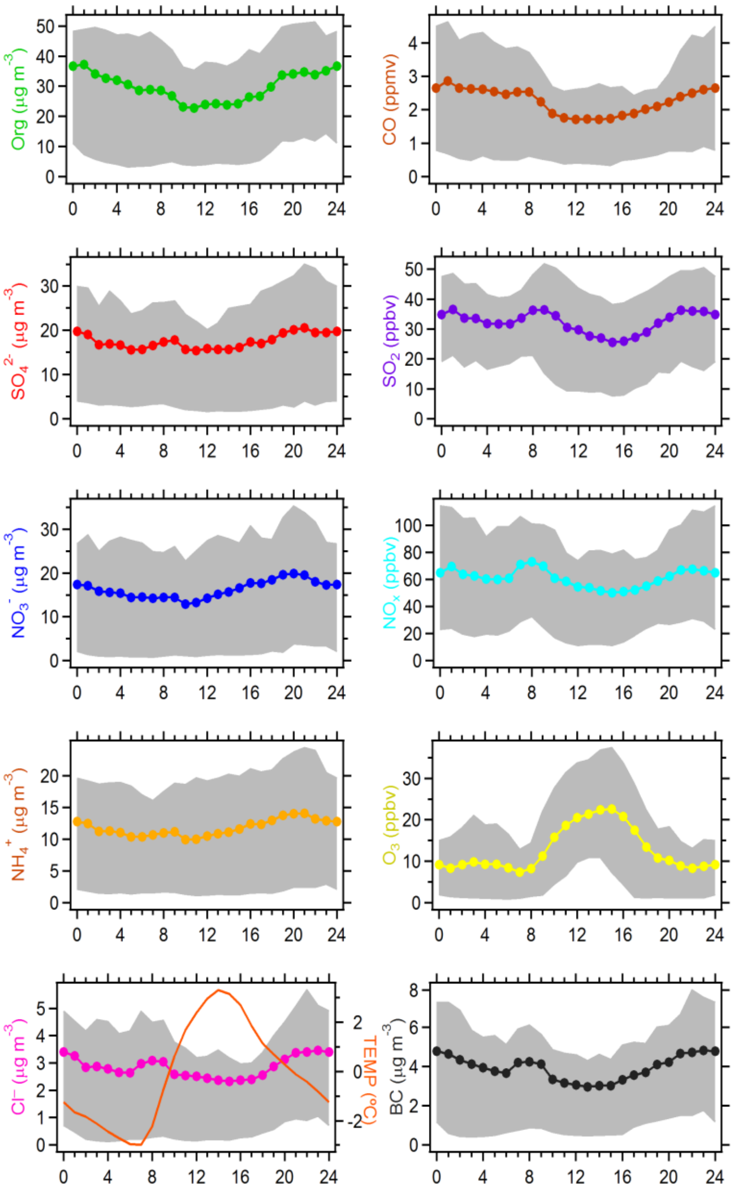

Figure S15. Diurnal patterns of chemical species of submicron particles and gaseous pollutants during the winter observation. The shaded area is between the 25% and 75% quantiles.

During four seasons, NOR ($\boldsymbol{n}$–NO_3^-/ ($\boldsymbol{n}$–NO_3^-+ $\boldsymbol{n}$–NO_2)) showed strong correlations with NH_4^+, indicating the main form of NO_3^- was NH_4NO_3. NH_4^+ also presented in the form of $(NH_4)_2SO_4$ and NH_4Cl. The predicted NH_4^+ was calculated assuming full neutralization of particulate anions of NO_3^-, SO_4^{2-}, and Cl^- in four seasons. The slopes of linear fitting of measured against predicted NH_4^+ in spring, summer, autumn and winter were 1.05, 1.02, 0.85, and 0.89, respectively. In autumn and winter, the relatively lower slopes implied that NH_4^+ was not enough to balance NO_3^-, SO_4^{2-} and Cl^-.

Field and emission studies have shown that a large fraction of KCl can exist in the fresh biomass burning plumes. As biomass burning plumes get aged, more S- and N- containing species (e.g., KNO_3 and K_2SO_4) in aerosol phase have been found (Li et al., 2003; Yokelson et al., 2009). It has also been reported that NaCl and NH_4Cl are important components in the aerosols directly emitted from biomass burning (Lewis et al., 2009; Levin et al., 2010). It was found that atmospheric aerosols were mostly acidic during heavy pollution episodes (Zhang et al, 2007; Sun et al, 2014.). During the heavy pollution periods in winter, SO_4^{2-} may exist in the form of NH_4HSO_4. Chloride existing in the form of KCl and NaCl in aerosol phase for coal combustion sources has been reported (McNallan et al., 1981; Doshi et al., 2009). Therefore, NO_3^-, SO_4^{2-}, and Cl^- may exist as other forms in addition to ammonium due to the influences of intense autumn biomass burning and coal combustion in autumn and winter, respectively.

Table S3. Concentrations of main chemical components in PM_1 during seasonal observations in Beijing in recent years. Unit: μg m^{-3}.

Seasons	**Periods**	**PM_1**	**OA**	**SO_4^{2-}**	**NO_3^-**	**NH_4^+**	**Cl^-**	**BC**	**References**
Spring	10 Apr.-4 May. 2008	87.0	39.0						Zhang et al., 2013
	30 Mar.-7 May. 2012	**45.1**	**14.0**	**9.3**	**10.2**	**7.3**	**1.2**	**3.1**	**This study**
Summer	9-21 Jul. 2006	80.0	28.1	20.3	17.3	13.1	1.1		Sun et al., 2010
	24 Jul.-20 Sept. 2008	63.1	23.9	16.8	10.0	10.0	0.5	1.8	Huang et al., 2010
	5 Jun.-3 Jul. 2008	94.0	34.0	24.8	20.1	13.7	1.4		Zhang et al., 2013
	26 Jun.-28 Aug. 2011	50.0	20.0	9.0	12.4	8.0	0.5		Sun et al., 2012
	4 Aug.-14 Sept. 2011	84.3	26.4	22.0	16.8	13.7	1.0	4.4	Hu et al., 2016
	29 Jul.-29 Aug. 2012	**37.5**	**12.5**	**9.7**	**6.4**	**5.4**	**0.4**	**3.2**	**This study**
Autumn	4-18 Oct. 2008	51.0	24.0	8.1	12.0	6.2	0.7		Zhang et al., 2013
	1-30 Sept. 2012	40.9	17.1	6.4	8.1	5.1	0.5	3.7	Jiang et al., 2013
	13 Oct.-13 Nov. 2012	**41.3**	**18.2**	**5.5**	**7.9**	**4.5**	**2.0**	**3.2**	**This study**
Winter	4 Jan.-3 Feb. 2008	73.0	43.0	11.4	9.2	6.4	3.5		Zhang et al., 2013
	22 Nov.-22 Dec. 2010	69.5	34.5	8.7	6.8	7.7	5.8	6.0	Hu et al., 2016
	14 Dec. 2010-15 Jan. 2011		20.9						Liu et al., 2012
	21 Nov. 2011-20 Jan. 2012	66.8	34.4	9.4	10.7	8.7	3.3		Sun et al., 2013
	1-17 Jan. 2013	83.0	38.3	14.3	12.5	9.2	2.6	6.0	Sun et al., 2014
	1 Jan.-1 Feb. 2013	89.3	44.7	19.6	12.5	8.9	3.6		Zhang et al., 2014
	23 Jan.- 2 Mar. 2013	**81.7**	**29.7**	**17.4**	**16.2**	**11.7**	**2.8**	**3.9**	**This study**

S5 Determination of the PMF solution

Factor number from 1 to 10 and the different seeds (0-50) were selected to run in the PMF model. For the spring observation, diagnostic plots of the PMF analysis are shown in Fig. S16. When OA was separated into four fractions, it included more oxidized (MO-OOA) and less oxidized OOA (LO-OOA), cooking OA (COA) and hydrocarbon-like OA (HOA). The performances of spectra and time series of the four factors at different f_{peak} are shown in Fig. S17. When OA was separated into five fractions, OOA was also split into two factors, but more information on the OA sources (BBOA) could be provided. When more than five factors, OOA decomposed into three or more factors. After comparing the performances of MS spectra and time series of five factors at different f_{peak}, the five factors, f_{Peak}=1 solution is chosen as the optimal solution for this PMF analysis because the signal of the characteristic ion fragment m/z is more obvious in one factor. In the five-factor solution, the mass spectra of two OOA factors are similar (r= 0.955), and the elemental ratios and OA/OC ratios (O/C: 0.99, 1.00; H/C: 1.50, 1.26; OA/OC: 2.51, 2.47) are close. It is unclear if the two OOA components represent distinct sources or chemical types. Thus, two OOA factors were combined into total OOA for further analysis (Hayes et al., 2013). Finally, four factors of OA were obtained, i.e., oxygenated OA (OOA), cooking OA (COA), hydrocarbon-like OA (HOA), and biomass burning OA(BBOA), as shown in Fig. S28. The detailed information on how to select the optimum PMF solution is available in Table S4.

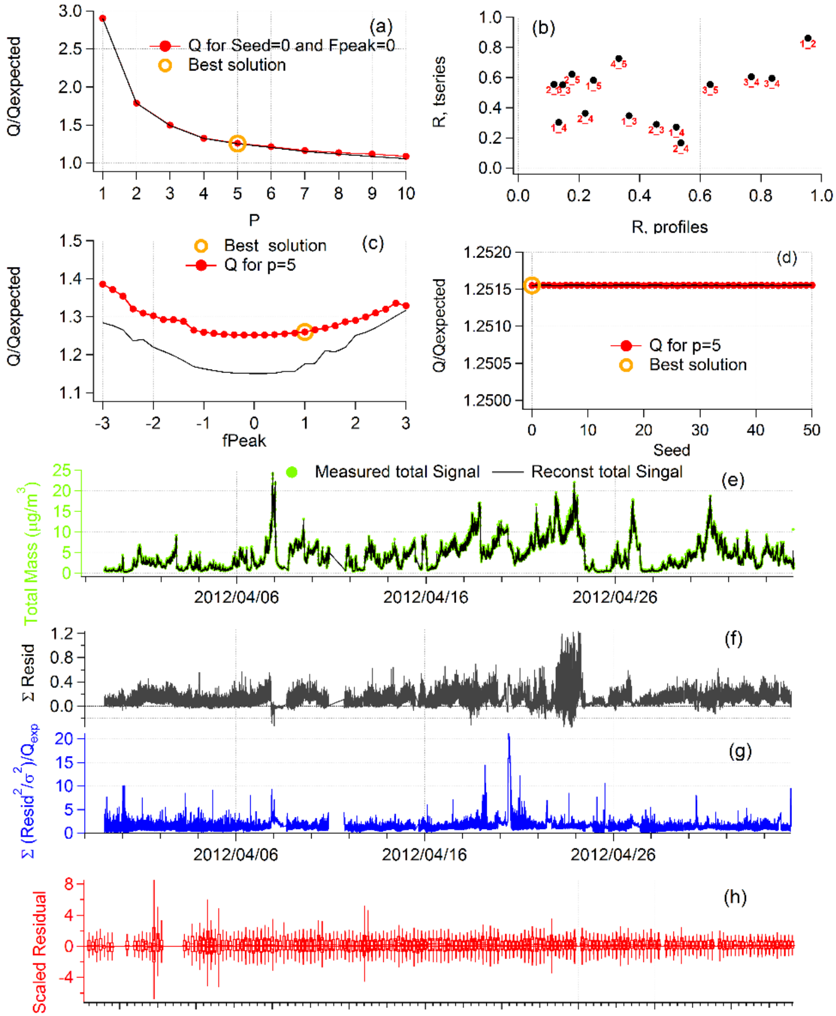

Figure S16. Diagnostic plots of the PMF analysis on OA mass spectral matrix for the spring observation.

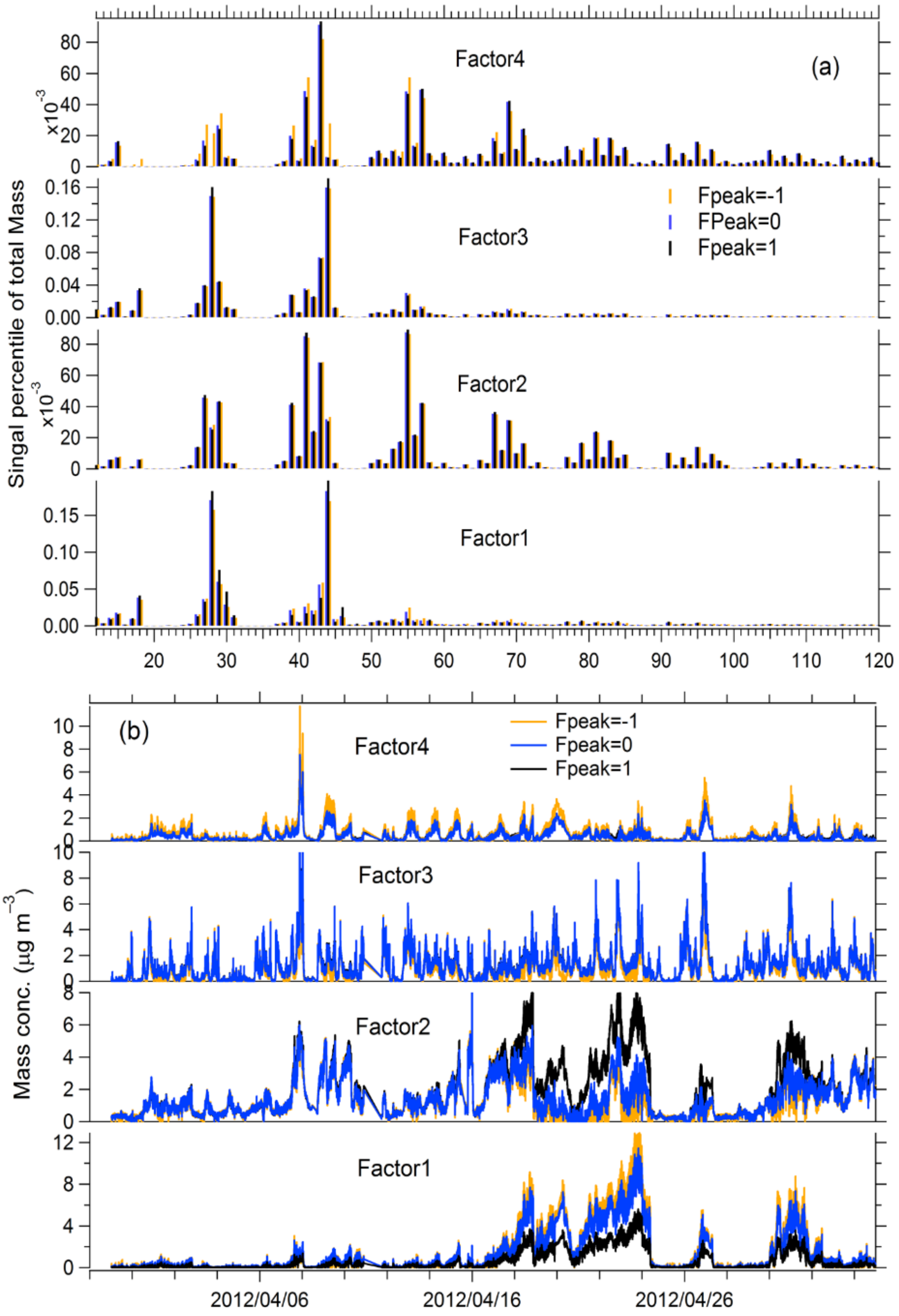

Figure S17. The spectra and time series of 4-factor solution at different f_{peak} values for the spring observation.

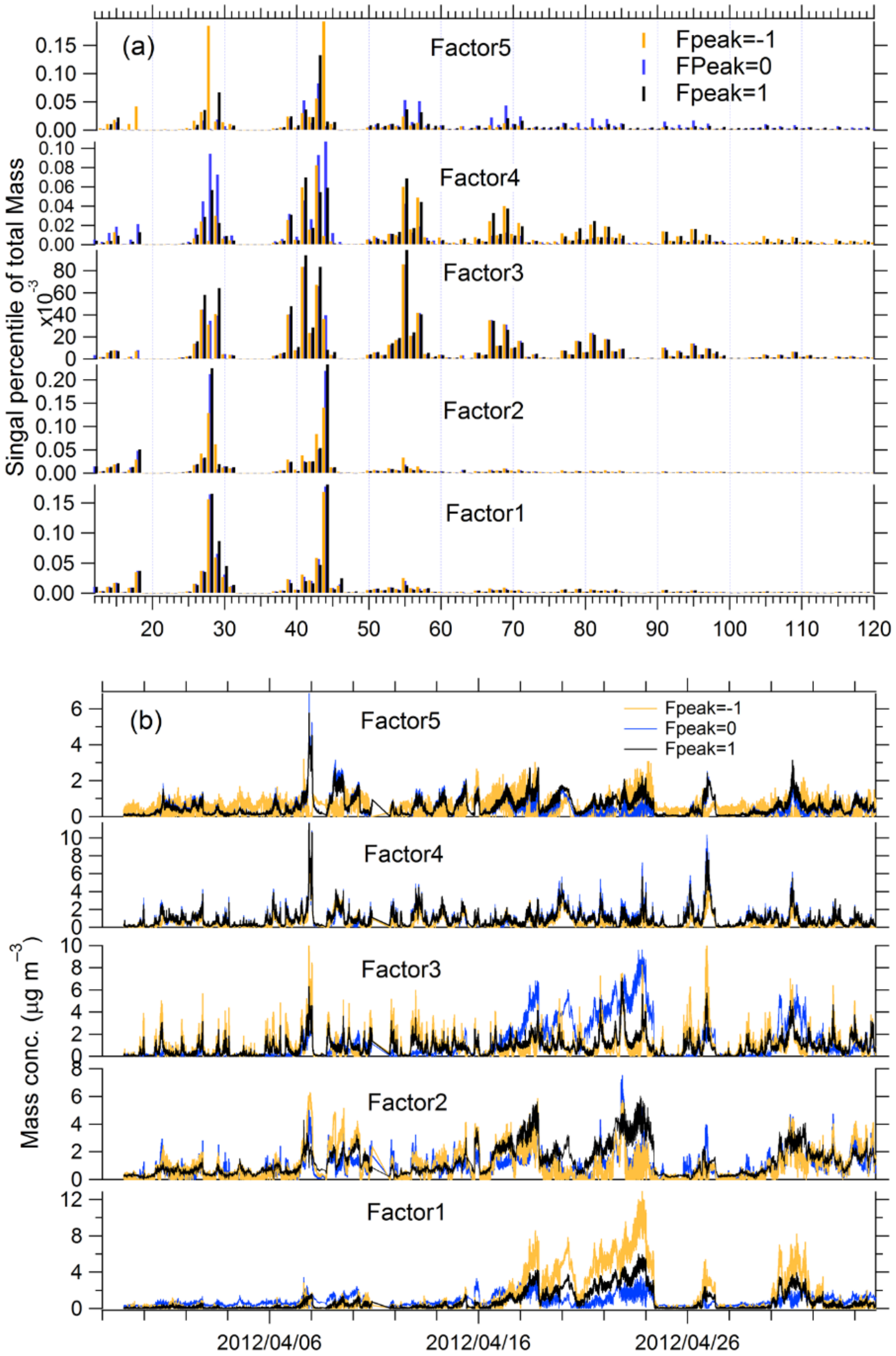

Figure S18. The spectra and time series of 5-factor solution at different f_{peak} values for the spring observation.

Table S4 Descriptions of PMF solutions for the spring observation in Beijing.

Factor number	F_{peak}	Seed	Q/Q_{exp}	Solution Description
1	0	0	2.90	Too few factors, large residuals at time periods and key *m/z*'s
2	0	0	1.79	Too few factors, large residuals at time periods and key *m/z*'s
3	0	0	1.49	Too few factors (OOA, HOA and COA). The Q/Q_{exp} at different seeds (0-50) are very unstable. Factors are mixed to some extent based on the time series and spectra.
4	0	0	1.32	OA factors could be identified as MO-OOA, LO-OOA, COA and HOA. Time series and diurnal variations of OA factors are consistent with the external tracers. But, the signal of characteristic ion *m/z* 60 biomass burning is strong in HOA factor.
5	**1**	**0**	**1.25**	**Final choice for the PMF solution. Two OOA factors, COA, HOA and BBOA are identified. Two similar OOA factors are combined for further analysis. Time series and diurnal variations of OA factors are consistent with the external tracers.**
6-10	0	0	1.20-1.06	Factor split. OOA was split into three or more factors with similar spectra, however, different time series.
5	-3 to 3	0	1.25-1.39	In f_{peak} range from −1.0 to 1.0, factor MS of OOA and COA are nearly identical, but there is a shift between HOA and BBOA for some ion fragments. The time series of OOA and HOA are nearly identical, but the other show some changes.

For the summer observation, the 4-factor, f_{peak}=0 solution was selected as the optimum solution. Four OA factors are more oxidized (MO-OOA) and less oxidized OOA (LO-OOA), cooking OA (COA) and hydrocarbon-like OA (HOA). The performances of spectra and time series of the four factors at different f_{peak} were also investigated. The detailed information on how to select the optimum PMF solution can be found in Figure S19-S21 and Table S5.

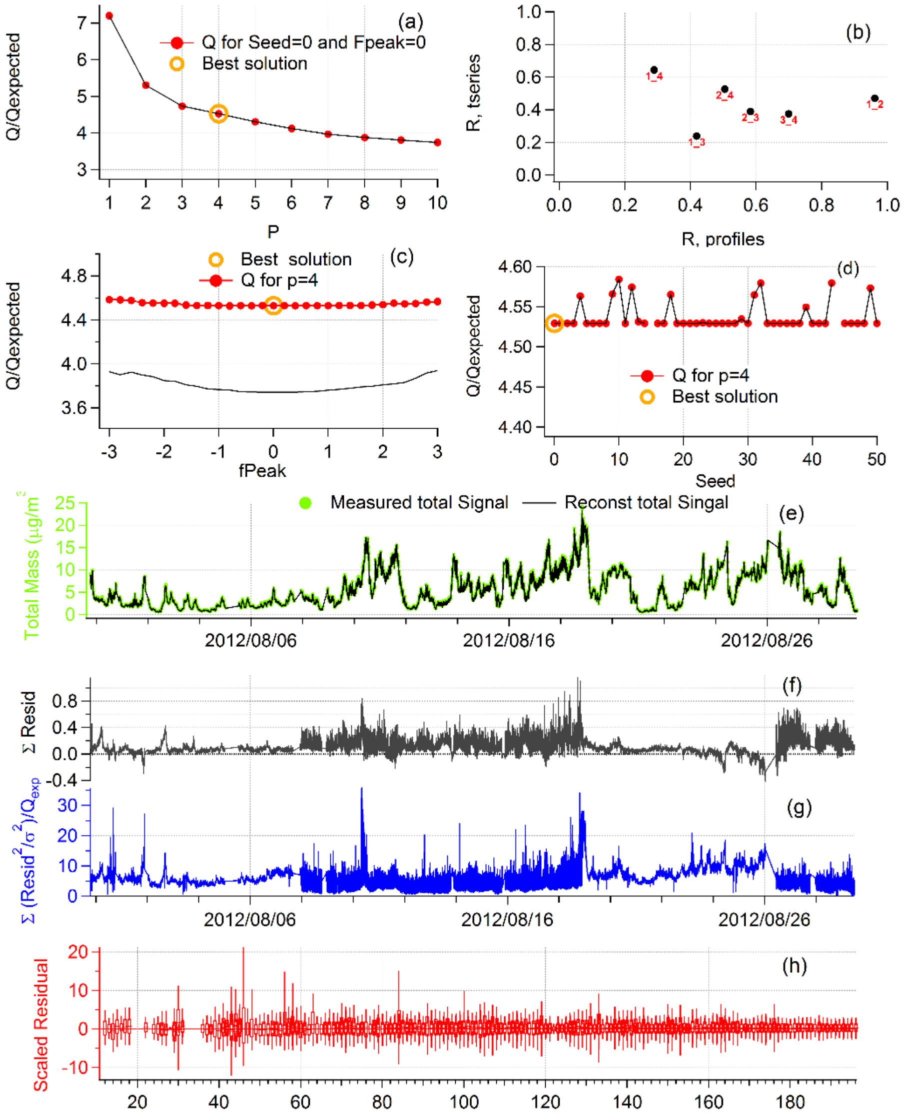

Figure S19. Diagnostic plots of the PMF analysis on OA mass spectral matrix for the summer observation.

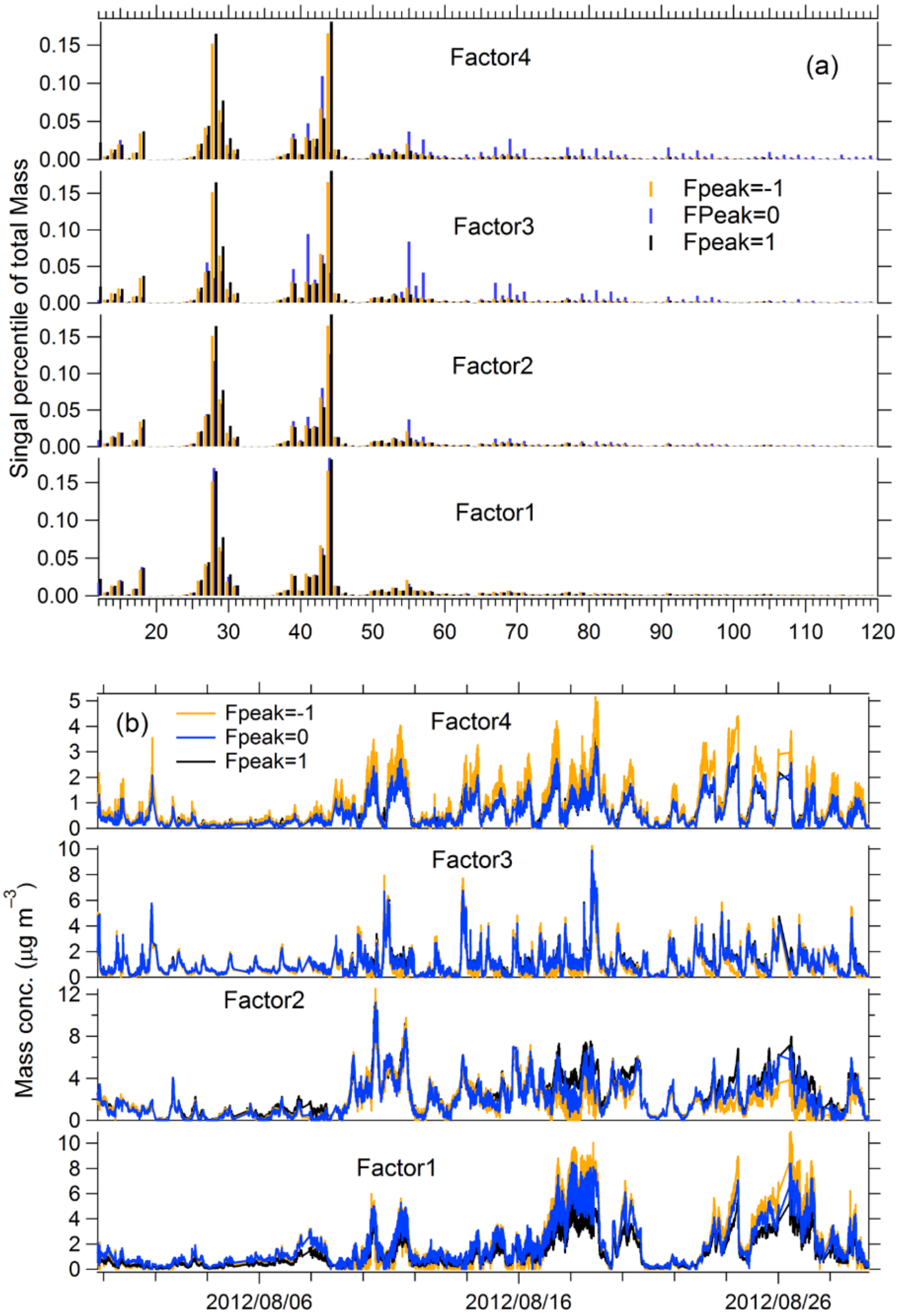

Figure S20. The spectra and time series of 4-factor solution at different f_{peak} values for the summer observation.

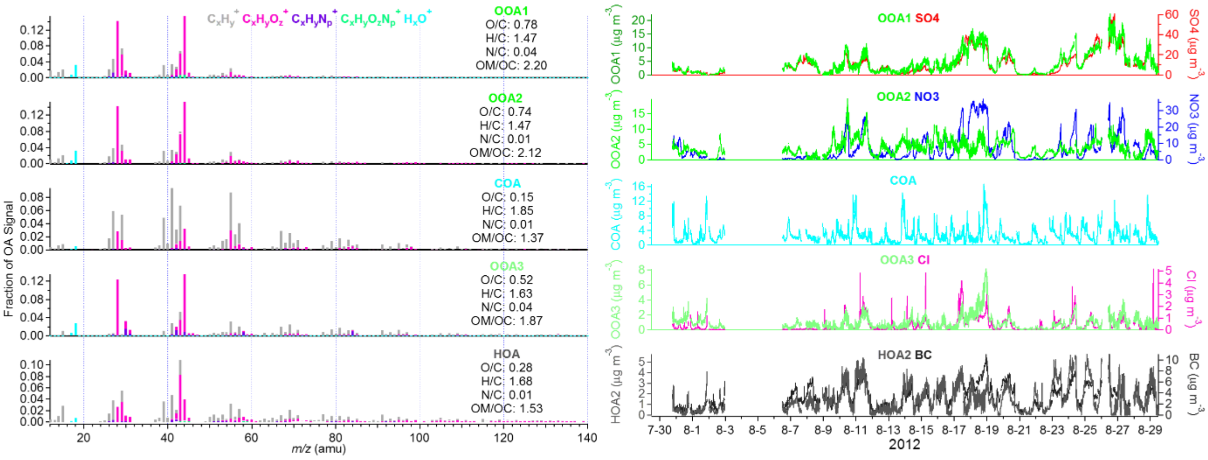

Figure S21. Unit mass spectra and time series of OA factors for 5-factor solution. The factors are marked as OOA1, OOA2, COA, OOA3 and HOA, respectively. OOA1, OOA2 and OOA3 show similar MS features (r=0.87–0.90). It is unclear if these OOA components represent distinct sources or chemical types. The elemental ratios and OA/OC ratios of each component are added.

Table S5 Descriptions of PMF solutions for the summer observation in Beijing.

Factor number	Fpeak	Seed	Q/Q_{exp}	Solution Description
1	0	0	7.20	Too few factors, large residuals at time periods and key *m/z*'s
2	0	0	5.31	Too few factors, large residuals at time periods and key *m/z*'s
3	0	0	4.73	Too few factors (OOA, HOA and COA). Factors are mixed to some extent based on the time series and spectra.
4	**0**	**0**	**4.53**	**Optimum solution for the PMF analysis (MO-OOA, LO-OOA, COA and HOA). Time series and diurnal variations of OA factors are consistent with the external tracers. The spectra of four factors are consistent with the source spectra in AMS spectra database.**
5-10	0	0	4.30-3.74	Factor split. Take 5 factor number solution as an example, OOA is likely split into three factors with similar mass spectra and different time series. However, it is difficult to explain if they represent distinct sources or chemical types.
4	-3 to 3	0	4.53-4.58	In f_{peak} range from −1.0 to 1.0, factor MS and time series are nearly identical.

The solution of the PMF analysis for the autumn observation is similar to that for the spring observation. When OA was separated into five fractions, OOA was also split into two factors, but a BBOA factor of distinct characteristics (f_{60}=1.3%) could be identified. When more than five factors, OOA decomposed into three or more factors. The performances of spectra and time series of the four factors at different f_{peak} are nearly identical. The five factors, f_{Peak}=0 and seed=0 solution is chosen as the optimal solution for this PMF analysis. In the five-factor solution, two OOA factors have similar MS characteristics (r= 0.976) and the elemental ratios and OA/OC ratios (O/C: 0.85−0.91; H/C: 1.24−1.40; OA/OC: 2.24−2.37) are close. It is unclear if the two OOA components represent distinct sources or chemical types. Thus, two OOA factors were combined into total OOA for further analysis (Hayes et al., 2013). Finally, four factors of OA were obtained, i.e., oxygenated OA (OOA), cooking OA (COA), hydrocarbon-like OA (HOA), and biomass burning OA(BBOA), as shown in Fig. S30. The detailed information on how to select the optimum PMF solution are given as Fig. S22-S24 and Table S6.

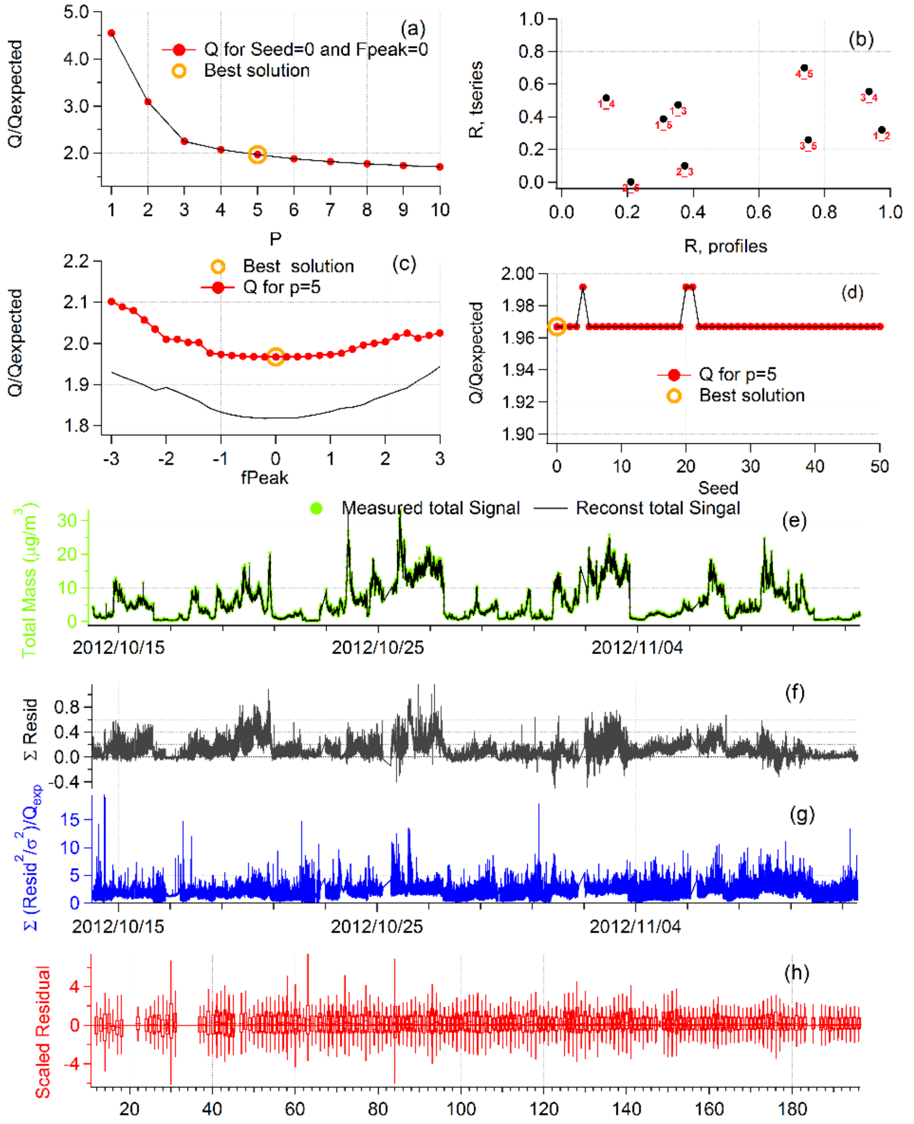

Figure S22. Diagnostic plots of the PMF analysis on OA mass spectral matrix for the autumn observation.

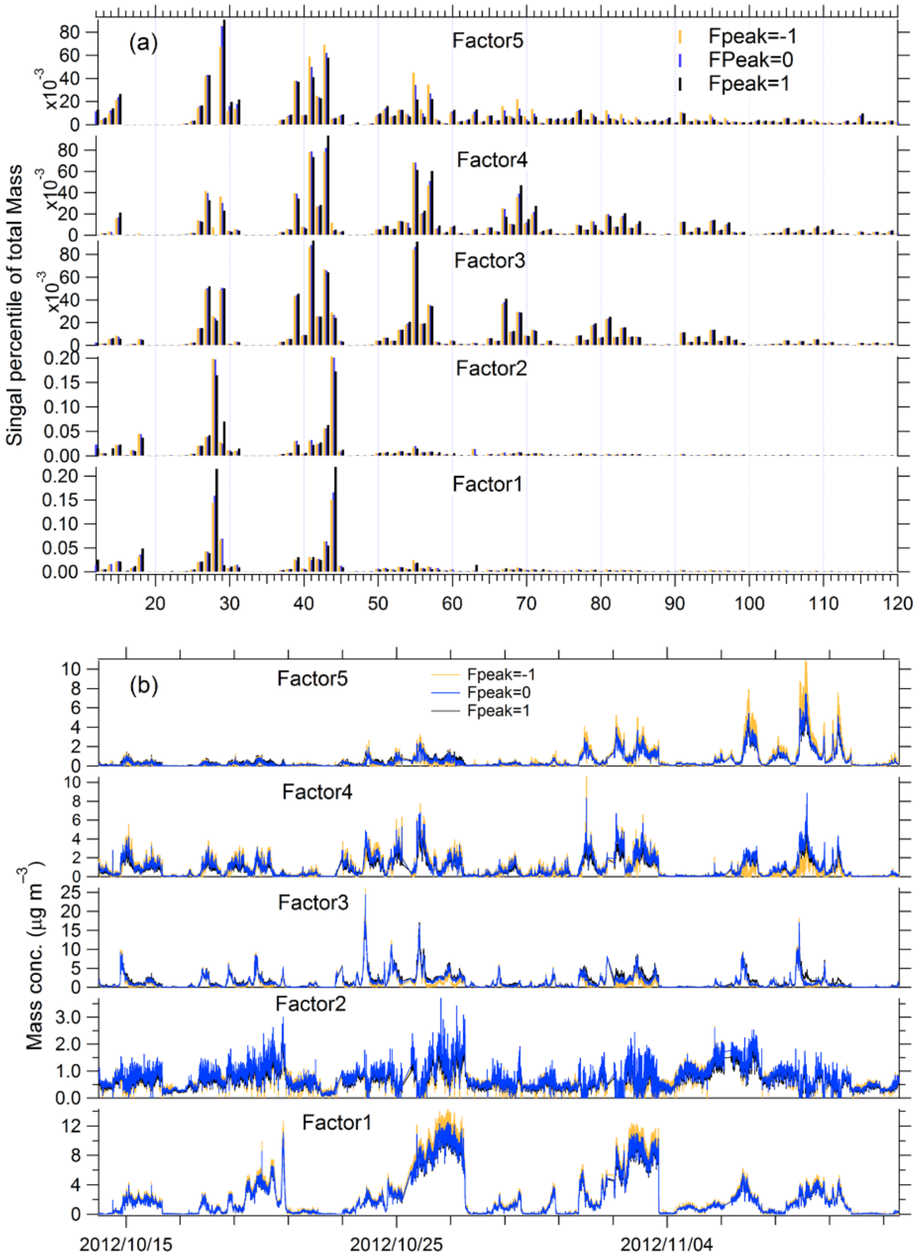

Figure S23. The spectra and time series of 5-factor solution at different f_{peak} values for the autumn observation.

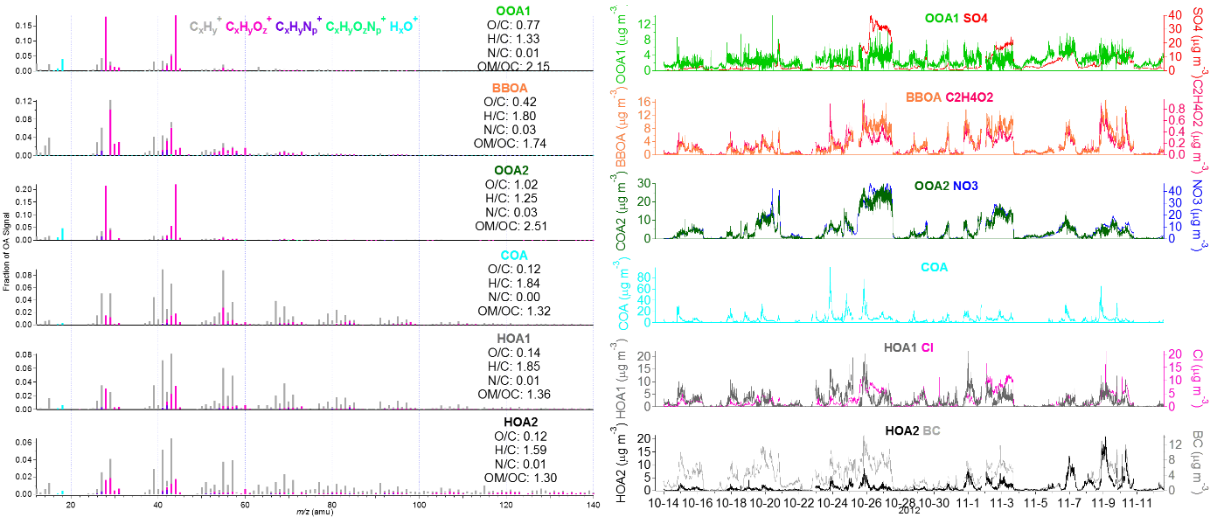

Figure S24. Unit mass spectra and time series of OA factors for 6-factor solution. The factors are marked as OOA1, BBOA, OOA2, COA, HOA1 and HOA2, respectively. The time series of BBOA and OOA2 trend well (r=0.78). HOA1 and HOA2 have similar MS (r=0.94) and diurnal variations (r=0.93). These factors appear mixed with each other.

Table S6 Descriptions of PMF solutions for the autumn observation in Beijing.

Factor number	Fpeak	Seed	Q/Q_{exp}	Solution Description
1	0	0	4.55	Too few factors, large residuals at time periods and key *m/z*'s
2	0	0	3.09	Too few factors, large residuals at time periods and key *m/z*'s
3	0	0	2.25	Too few factors (OOA, COA and HOA). The Q/Q_{exp} at different seeds (0-50) are very unstable. The HOA factor contain high abundance (1.0%) of *m/z* 60.
4	0	0	2.07	Four factors include two similar OOA factors, COA and HOA. The HOA factor contain high abundance (1.1%) of *m/z* 60.
5	**0**	**0**	**1.97**	**Optimum solution for the PMF analysis (two OOA factor, COA, HOA and BBOA). Two similar OOA factors are combined for further analysis. Time series and diurnal variations of OA factors are consistent with the external tracers.**
6-10	0	0	1.88-1.71	Factor split. Some of the split factors have time series and MS that appear mixed.
5	-3 to 3	0	1.97-2.10	In f_{peak} range from −1.0 to 1.0, factor MS and time series are nearly identical.

For the winter observation, a 5-factor, f_{peak}=0 solution was selected as the optimum solution. Five OA factors are more oxidized (MO-OOA) and less oxidized OOA (LO-OOA), cooking OA (COA), coal combustion OA (CCOA) and hydrocarbon-like OA (HOA), respectively. The performances of spectra and time series of the five factors at different f_{peak} were also investigated. The detailed information on how to select the optimum PMF solution can be found in Fig. S25-S27 and Table S7.

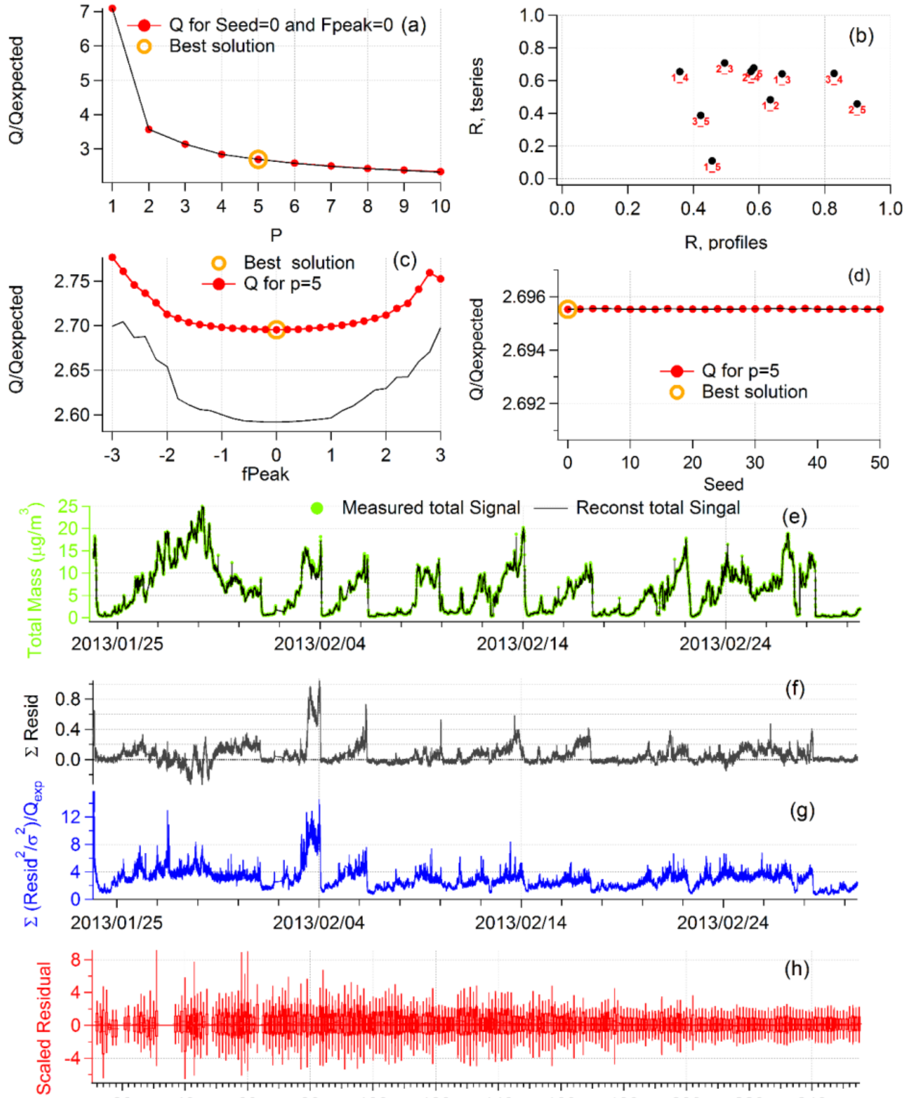

Figure S25. Diagnostic plots of the PMF analysis on OA mass spectral matrix for the winter observation.

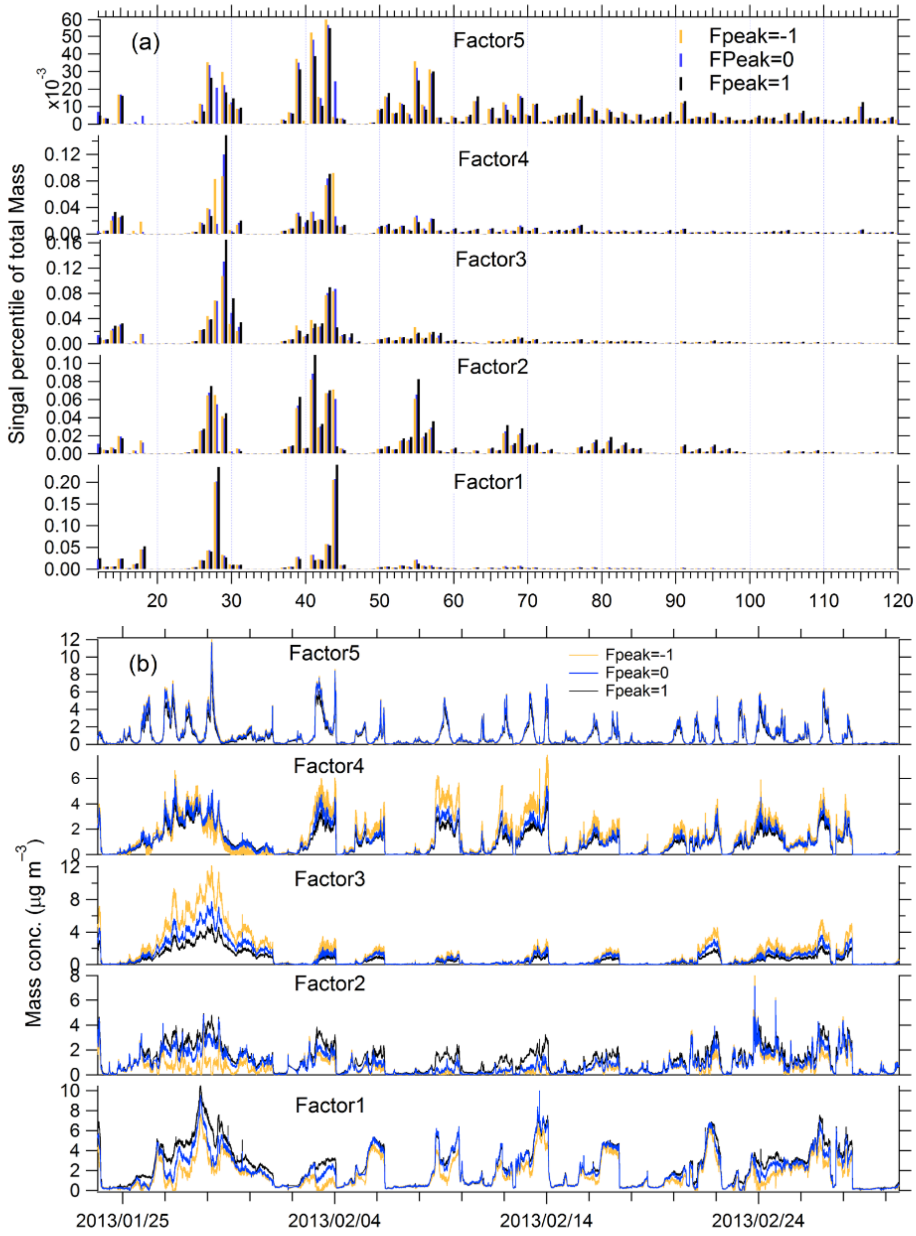

Figure S26. The spectra and time series of 5-factor solution at different f_{peak} values for the winter observation.

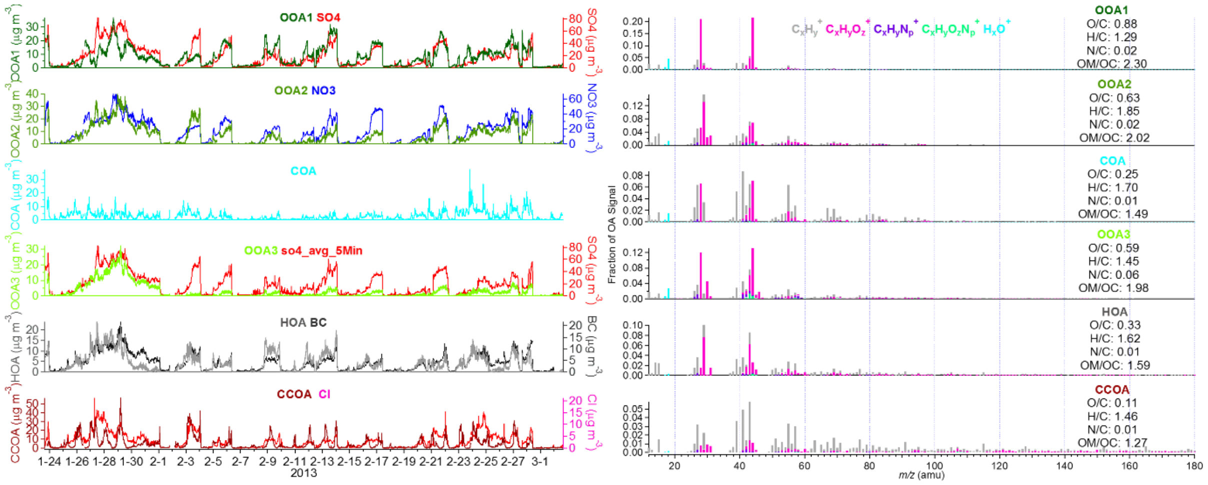

Figure S27. Unit mass spectra and time series of OA factors for 6-factor solution. The factors are marked as OOA1, OOA2, COA, OOA3, HOA and CCOA, respectively. OOA1, OOA2 and OOA3 show similar time series or MS features (r=0.56–0.95). The characteristics of OOA3 factor is not obvious. It is unclear if these factors represent distinct sources or chemical types.

Table S7 Descriptions of PMF solutions for the winter observation in Beijing.

Factor number	**Fpeak**	**Seed**	**Q/Q_{exp}**	**Solution Description**
1	0	0	7.09	Too few factors, large residuals at time periods and key *m/z*'s
2	0	0	3.57	Too few factors, large residuals at time periods and key *m/z*'s
3	0	0	3.14	Too few factors (OOA-, HOA- and COA-like). The Q/Q_{exp} at different seeds (0-50) are very unstable. Factors are mixed to some extent based on the time series and spectra.
4	0	0	2.84	OA is split to two OOA factors, COA and HOA. It seems that HOA mixed with CCOA.
5	**0**	**0**	**2.70**	**Optimum choice for PMF factors (MO-OOA, LO-OOA, COA, HOA and CCOA). Time series and diurnal variations of OA factors are consistent with the external tracers. The spectra of four factors are consistent with the source spectra in AMS spectra database.**
6-10	0	0	2.59-2.33	Factor split. Take 6 factor number solution as an example, OOA was split into three factors with similar spectra and/or time series.
5	-3 to 3	0	2.70-2.78	In f_{peak} range from −1.0 to 1, factor MS and time series are nearly identical, but there is likely a shift of the time series for LO-OOA and COA during the heavy-pollution episodes.

S6 Concentration and mass spectra of OA factors

Table S8. Resolved fractions of OA during seasonal observations in Beijing in recent years. Unit: µg m^{-3}.

Seasons	Periods	LV-OOA[a]	SV-OOA[b]	OOA	LSOA	RSOA	HOA	CCOA	COA	BBOA	OOA/OA (%)	References
Spring	10 Apr.-4 May. 2008			23.0			16.0				59	Zhang et al., 2013
	30 Mar.-7 May. 2012			**6.8**			**2.8**		**2.6**	**1.8**	**49**	This study
Summer	9-21 Jul. 2006	12.6	4.5				11.0				61	Sun et al., 2010
	24 Jul.-20 Sept. 2008	8.1	5.7				4.3		5.8		58	Huang et al., 2010
	5 Jun.-3 Jul. 2008			20.0			14.0				59	Zhang et al., 2013
	26 Jun.-28 Aug. 2011			12.7			7.1				64	Sun et al., 2012
	4 Aug.-14 Sept. 2011	9.7	7.4				3.4		5.5		66	Hu et al., 2016
	29 Jul.-29 Aug. 2012	**3.3**	**5.3**				**1.4**		**2.5**		**69**	This study
Autumn	4-18 Oct. 2008			11.0			13.0				46	Zhang et al., 2013
	1-30 Sept. 2012			12.5			4.6				73	Jiang et al., 2013
	13 Oct.-13 Nov. 2012			**8.6**			**2.5**		**5.2**	**2.0**	**47**	This study
Winter	4 Jan.-3 Feb. 2008			10.0			33.0				23	Zhang et al., 2013
	22 Nov.-22 Dec. 2010	6.2	4.3				4.7	8.2	6.7	4.1	30	Hu et al., 2016
	14 Dec.2010-15 Jan. 2011			4.9			5.6		10.4		23	Liu et al., 2012
	21 Nov. 2011-20 Jan. 2012			10.7			5.8	11.4	6.5		31	Sun et al., 2013
	1-17 Jan. 2013		8.9		7.8	4.7	5.3	7.3	4.8		55	Sun et al., 2014
	1 Jan.-1 Feb. 2013	12.5	11.6				4.9	6.7	8.9		54	Zhang et al., 2014
	23 Jan.- 2 Mar. 2013	**9.8**	**5.0**				**5.5**	**5.1**	**4.3**		**50**	This study

Note: In Hu et al. (2016) and this study, [a] LV-OOA is defined as more-oxidized oxygenated OA (MO-OOA); [b] SV-OOA is defined as less-oxidized oxygenated OA (LO-OOA).

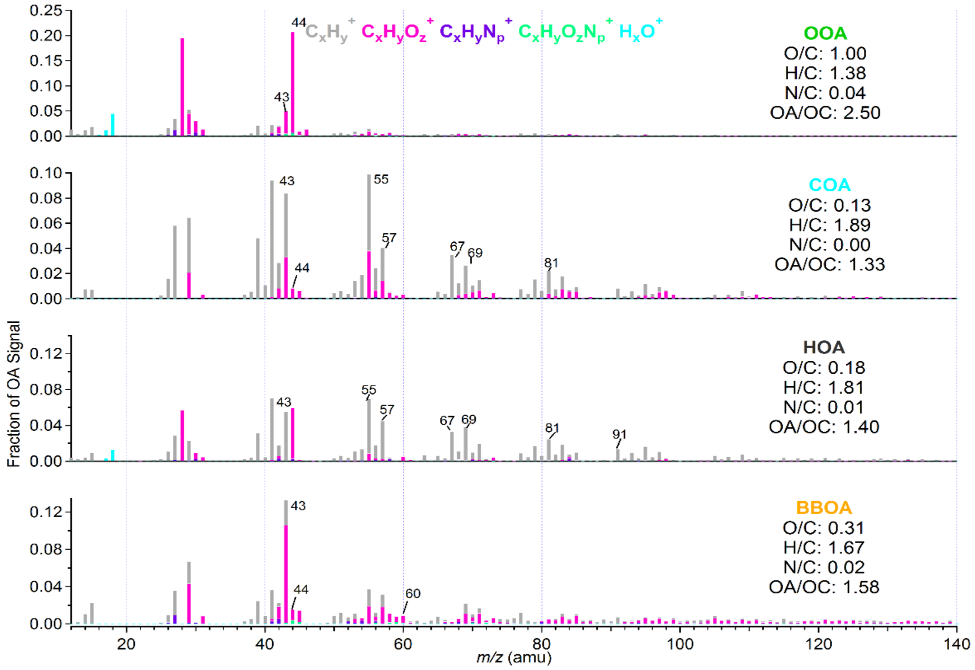

Figure S28. Unit mass spectra of OA factors resolved in the spring study: OOA, COA, HOA and BBOA. The elemental ratios and OA/OC ratios of each component are also shown in the legends. The ion fragments are classified into five categories to identify the mass spectra characteristics: $C_xH_y^+$, $C_xH_yO_z^+$, $C_xH_yN_p^+$, $C_xH_yO_zN_p^+$ and H_xO^+ represent the reductive alkyl fragments, the oxygenated fragments of carboxylic acid and aldehyde, the nitrogen-containing alkyl fragments, the oxygenated organonitrogen fragment ions, and fragmented H_2O and carboxyl, respectively.

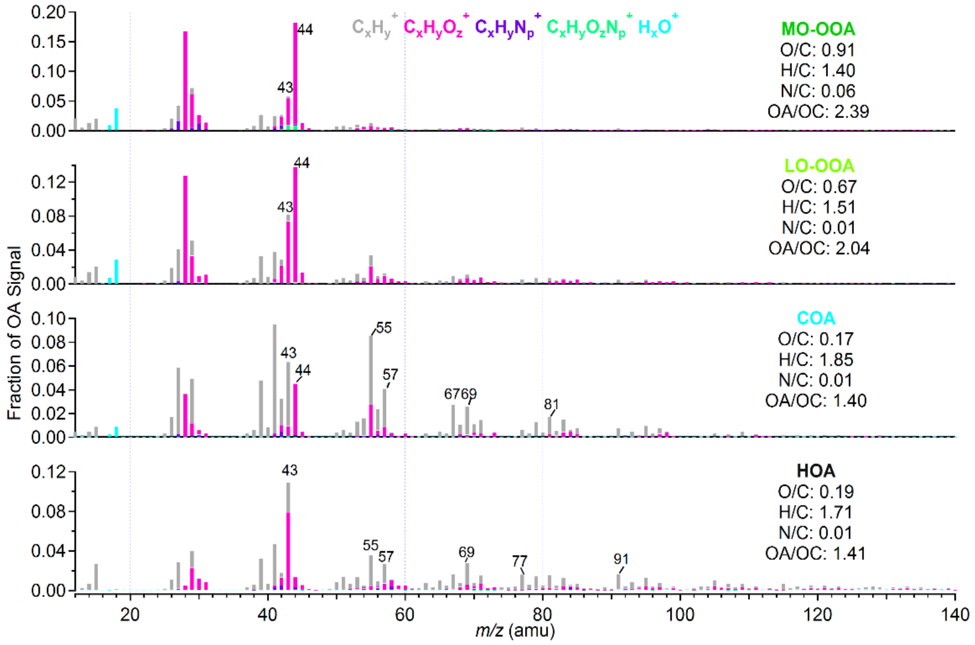

Figure S29. Unit mass spectra of OA factors resolved in the summer study: MO-OOA, LO-OOA, COA and HOA. The elemental ratios and OA/OC ratios of each component are also shown in the legends. The ion fragments are classified into five categories as described in Fig. S28.

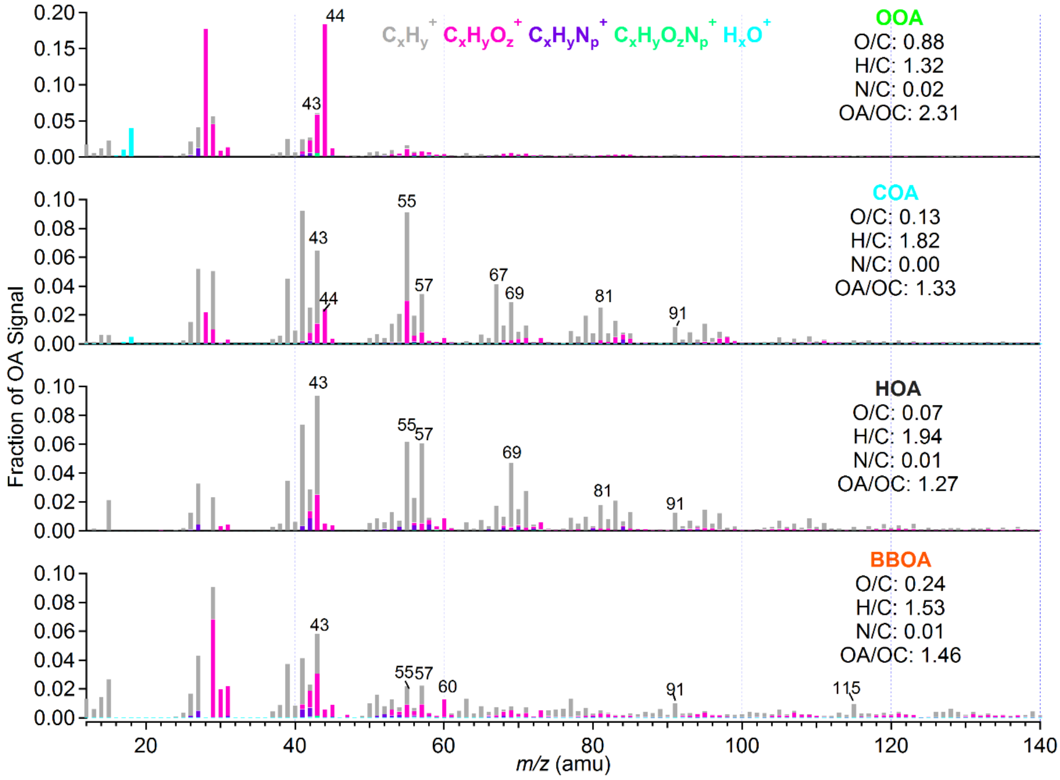

Figure S30. Unit mass spectra of OA factors resolved in the autumn study: OOA, COA, HOA, and BBOA. The elemental ratios and OA/OC ratios of each component are also shown in the legends. The ion fragments are classified into five categories as described in Fig. S28.

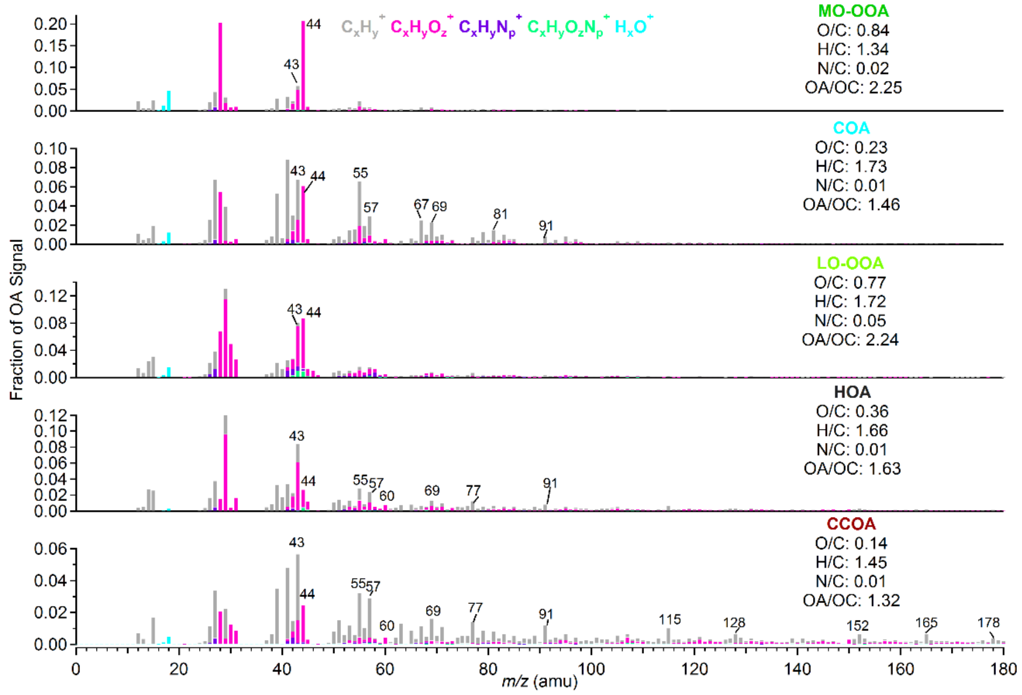

Figure S31. Unit mass spectra of OA factors resolved in the winter study: MO-OOA, LO-OOA, COA, HOA, and CCOA. The elemental ratios and OA/OC ratios of each component are also shown in the legends. The ion fragments are classified into five categories as described in Fig. S28.

S7 Time series of OA fractions

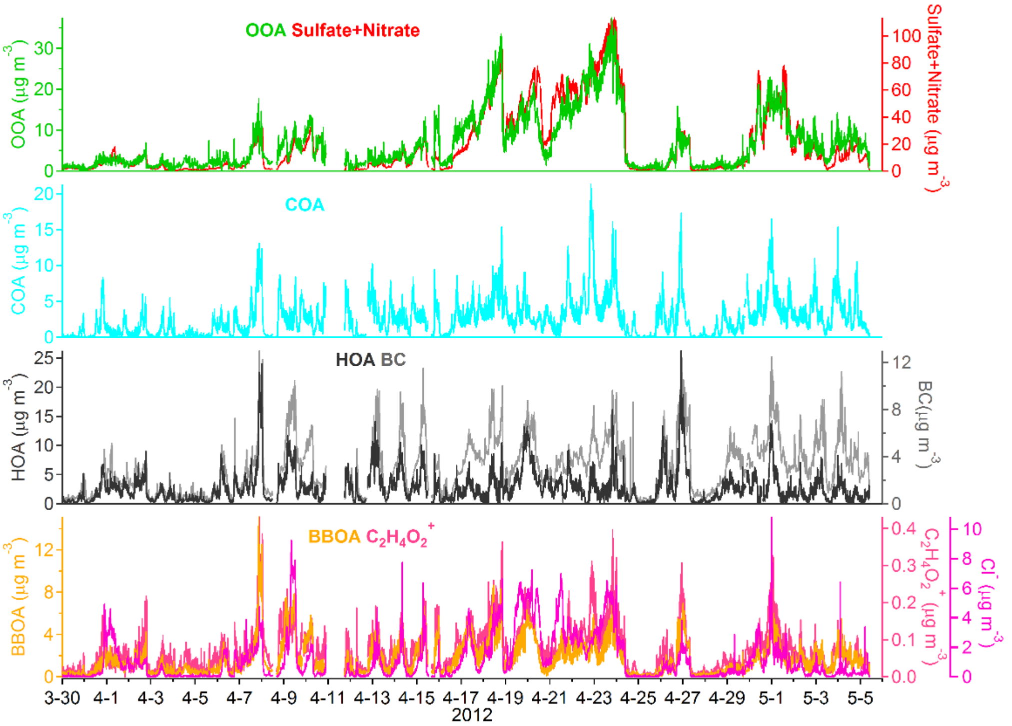

Figure S32. Time series of OA fractions and external tracers (sulfate, nitrate, chloride, BC, and $C_2H_4O_2^+$) during the spring observation.

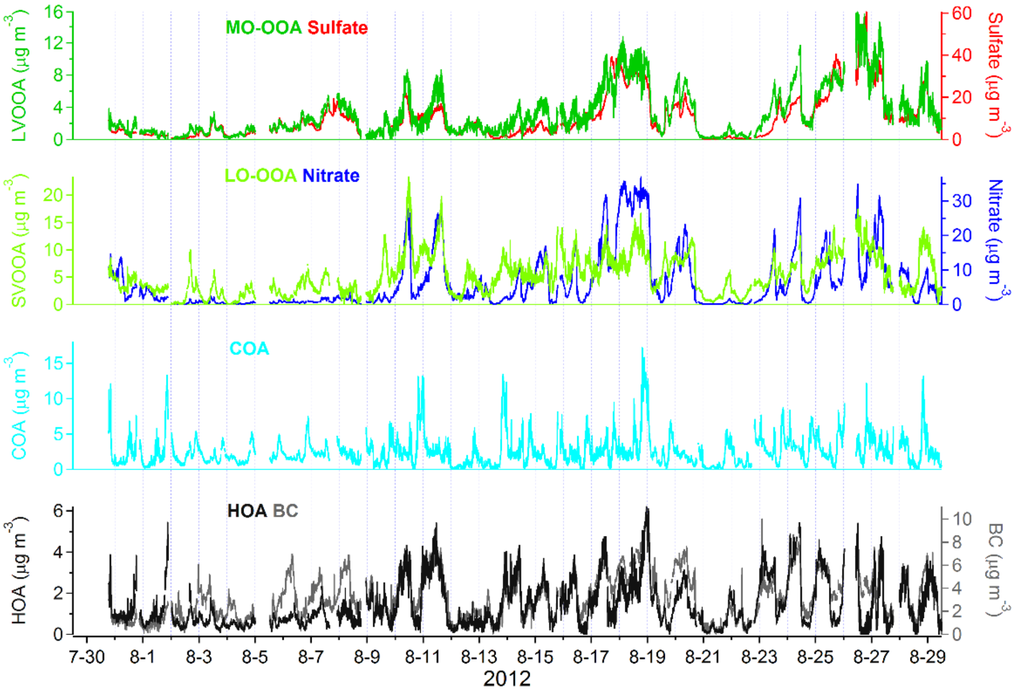

Figure S33. Time series of OA fractions and external tracers (sulfate, nitrate, and BC) during the summer observation.

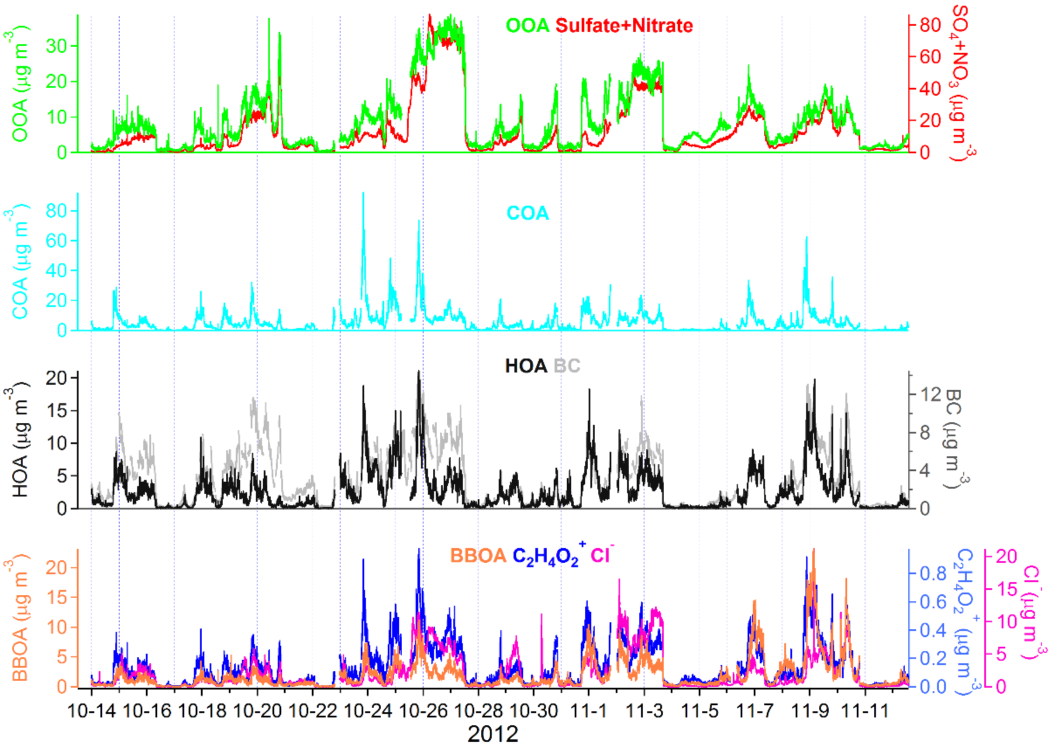

Figure S34. Time series of OA fractions and external tracers (sulfate+nitrate, BC, chloride and $C_2H_4O_2^+$) during the autumn observation.

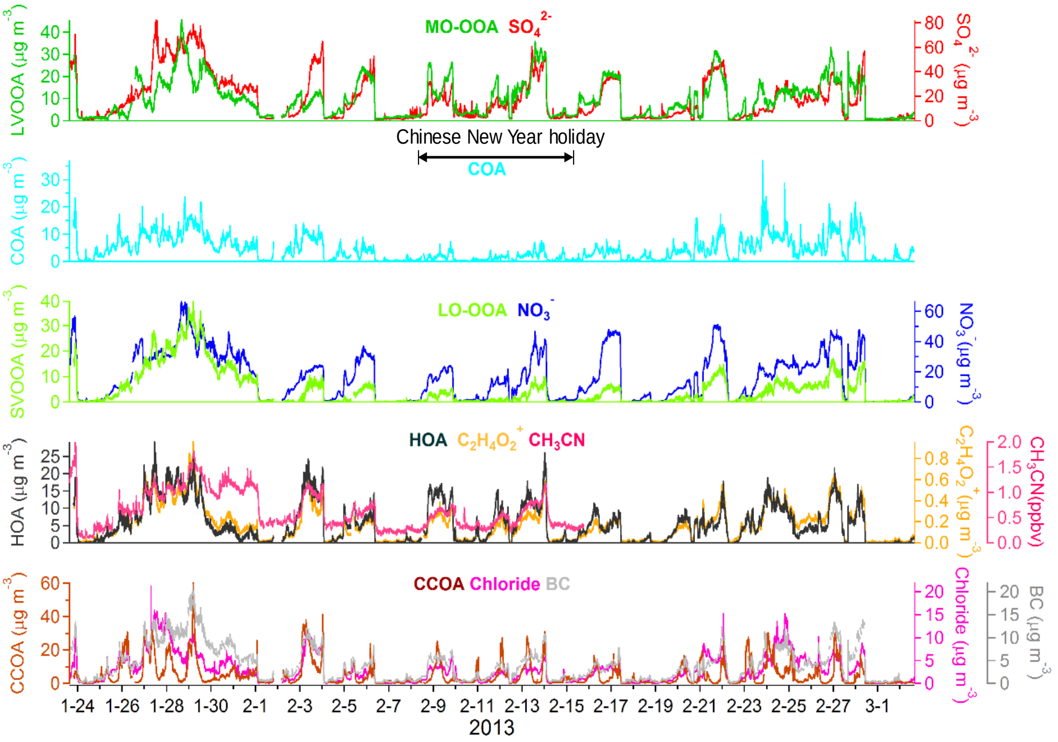

Figure S35. Time series of OA fractions and external tracers (sulfate, nitrate, $C_2H_4O_2^+$, acetonitrile, chloride and BC) during the winter observation.

S8 Elemental compositions of OA

The diurnal variations of element ratios (O/C, H/C) and OA/OC ratios were obvious during the seasonal observations in Beijing (Fig. S36-S39). The diurnal patterns of O/C and OA/OC ratios in the spring, summer and autumn were similar: during the daytime, the oxidation state of OA gradually increased due to the effect of photochemical reactions; the O/C and OA/OC ratios were peaked at about 16:00 in the afternoon, indicating that secondary formation is an important factor affecting the properties of OA. As the products of photochemical reactions, SOA gradually accumulated in the daytime, making an important contribution to OA. In the morning, the O/C and OA/OC ratios declined slightly at 7:00-8:00, which may be affected by reductive OA emitted from vehicles during the rush hour. They showed two valleys at noon (12:00-13:00) and in the evening (19:00-20:00), reflecting the impacts of cooking emissions during meal time (Huang et al., 2010). In the autumn, the oxidation state of OA (O/C and OA/OC ratio) maintained at a low level after the valley at 20:00, mainly caused by the biomass emissions at night. While in the summer, the O/C and OA/OC ratios rose after 20:00, indicating the aqueous oxidation processes may play a significant role under high humidity conditions at nighttime (Ervens et al., 2011). In the winter, the diurnal patterns of O/C and OA/OC ratios were close to those in other seasons, but the impacts of vehicular and cooking emissions were less significant than in other seasons; the oxidation state of OA kept to decrease after 20:00, which is mainly influenced by primary emissions (e.g., coal combustion and biomass burning) at night. Hydrogen mainly comes from the alkyl fragments. Along with oxidation of OA, alkyl functional groups are gradually substituted by oxygenated ones, the proportion of hydrogen in OA is gradually reduced. Therefore, the diurnal variations of H/C ratios always trended oppositely with those of O/C and OA/OC ratios.

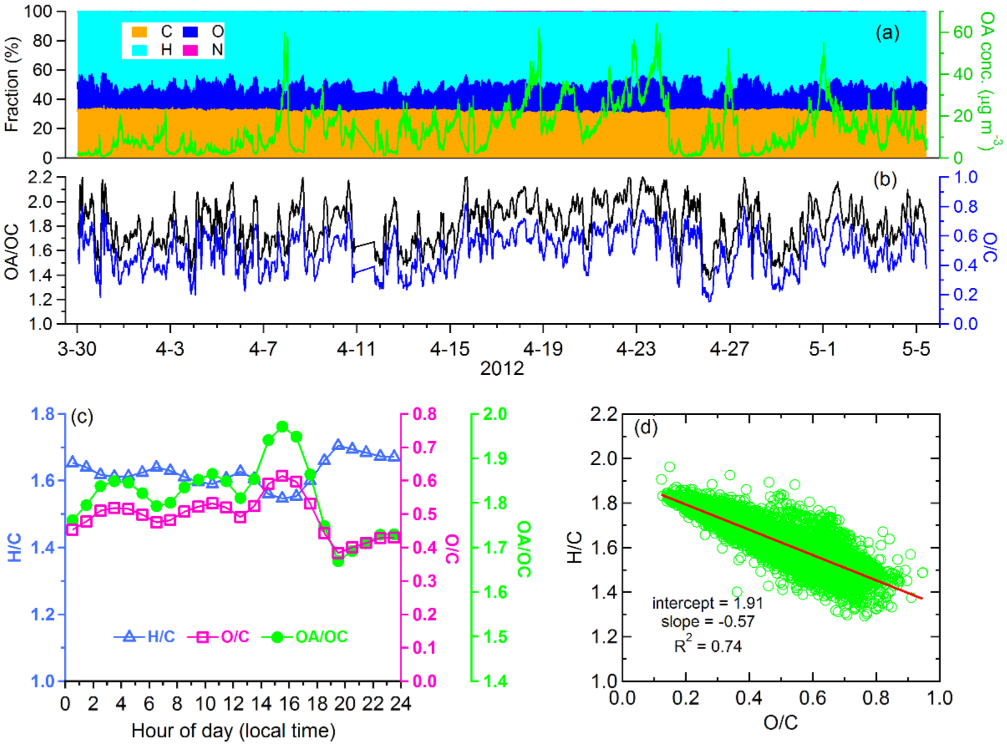

Figure S36. Time series of (a) elemental fractions and (b) OA/OC and O/C ratios in OA; (c) Diurnal patterns of OA/OC, H/C and O/C ratios; (d) van Krevelen diagram of OA during the spring observation.

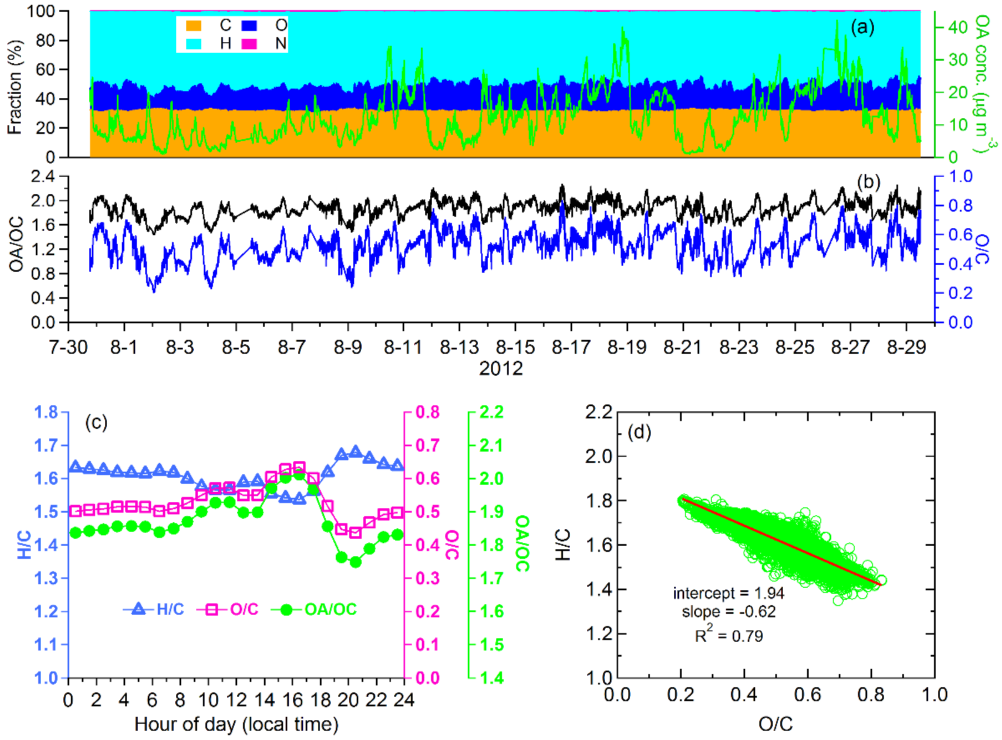

Figure S37. Time series of (a) elemental fractions and (b) OA/OC and O/C ratios in OA; (c) Diurnal patterns of OA/OC, H/C and O/C ratios; (d) van Krevelen diagram of OA during the summer observation.

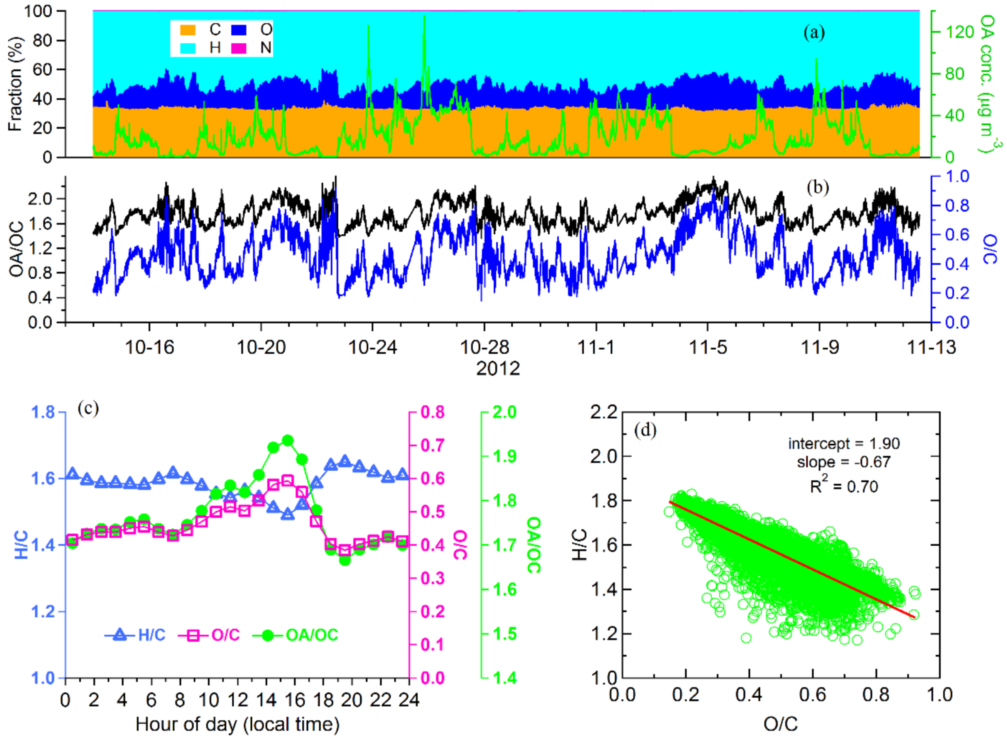

Figure S38. Time series of (a) elemental fractions and (b) OA/OC and O/C ratios in OA; (c) Diurnal patterns of OA/OC, H/C and O/C ratios; (d) van Krevelen diagram of OA during the autumn observation.

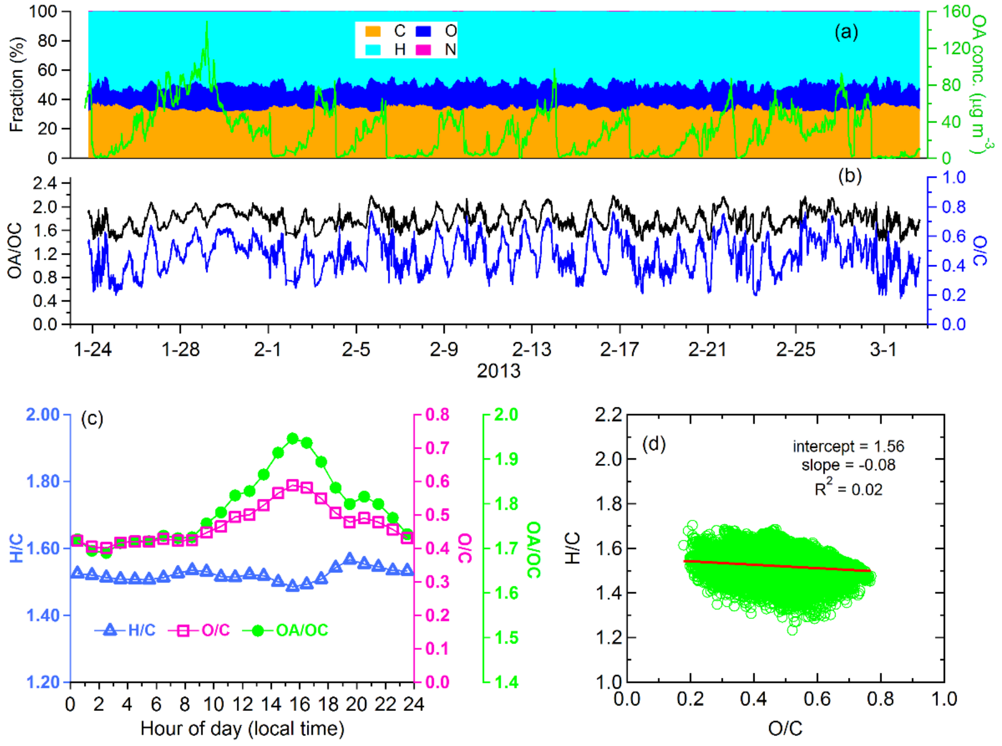

Figure S39. Time series of (a) elemental fractions and (b) OA/OC and O/C ratios in OA; (c) Diurnal patterns of OA/OC, H/C and O/C ratios; (d) van Krevelen diagram of OA during the winter observation.

S9 Correlation matrix of gaseous pollutants and particulate chemical compositions

Table S9 Correlation matrix of gaseous pollutants and particulate chemical compositions in submicron aerosols during the spring campaign.

	CO	NO_x	SO_2	O_3	O_x	SO_4^{2-}	NO_3^-	NH_4^+	Cl^-	BC	$C_2H_4O_2^+$	OOA	COA	HOA	BBOA
CO	1.000														
NO_x	.475	1.000													
SO_2	**.755**	.301	1.000												
O_3	-.376	-.679	-.051	1.000											
O_x	.219	.029	.485	.561	1.000										
SO_4^{2-}	**.758**	.189	.531	-.205	.186	1.000									
NO_3^-	**.773**	.361	.550	-.314	.258	**.871**	1.000								
NH_4^+	**.798**	.300	.577	-.282	.231	**.953**	**.973**	1.000							
Cl^-	**.764**	.480	.598	-.461	.094	**.667**	**.755**	**.771**	1.000						
BC	**.615**	**.826**	.513	-.532	.275	.454	**.635**	.580	**.676**	1.000					
$C_2H_4O_2^+$	.591	.580	.448	-.396	.342	.556	**.716**	**.670**	**.674**	**.822**	1.000				
OOA	**.704**	.274	.542	-.196	.346	**.881**	**.925**	**.936**	**.668**	.570	**.705**	1.000			
COA	.464	.439	.309	-.241	.429	.486	.537	.524	.371	.584	**.754**	**.603**	1.000		
HOA	.432	**.787**	.272	-.572	.106	.136	.325	.260	.497	**.728**	**.691**	.231	.560	1.000	
BBOA	.548	.596	.497	-.422	.285	.454	**.624**	.578	**.705**	**.819**	**.831**	**.652**	.538	**.695**	1.000

Table S10 Correlation matrix of gaseous pollutants and particulate chemical compositions in submicron aerosols during the summer campaign.

	CO	NO_x	SO_2	O_3	O_x	SO_4^{2-}	NO_3^-	NH_4^+	Cl^-	BC	$C_2H_4O_2^+$	LV-OOA	SV-OOA	COA	HOA
CO	1.000														
NO_x	.456	1.000													
SO_2	.354	-.027	1.000												
O_3	-.041	-.541	.382	1.000											
O_x	.124	-.310	.431	.957	1.000										
SO_4^{2-}	.620	.099	.644	.261	.351	1.000									
NO_3^-	.718	.334	.321	-.123	-.007	.657	1.000								
NH_4^+	.720	.213	.555	.098	.205	.932	.882	1.000							
Cl^-	.625	.441	.186	-.252	-.145	.463	.795	.668	1.000						
BC	.773	.672	.270	-.232	-.030	.604	.740	.715	.727	1.000					
$C_2H_4O_2^+$	.697	.469	.327	.030	.227	.667	.702	.737	.619	.773	1.000				
MO-OOA	.663	.260	.529	.129	.252	.912	.813	.946	.651	.756	.745	1.000			
LO-OOA	.601	.196	.320	.382	.543	.642	.626	.682	.449	.613	.816	.691	1.000		
COA	.428	.449	.100	-.135	.035	.266	.238	.274	.217	.415	.646	.222	.310	1.000	
HOA	.558	.741	.036	-.404	-.203	.255	.626	.443	.710	.787	.705	.498	.469	.423	1.000

Table S11 Correlation matrix of gaseous pollutants and particulate chemical compositions in submicron aerosols during the autumn campaign.

	CO	NO_x	SO_2	O_3	O_x	SO_4^{2-}	NO_3^-	NH_4^+	Cl^-	BC	$C_2H_4O_2^+$	OOA	COA	HOA	BBOA
CO	1.000														
NO_x	.639	1.000													
SO_2	.694	.379	1.000												
O_3	-.511	-.694	-.319	1.000											
O_x	.517	.371	.566	-.044	1.000										
SO_4^{2-}	.789	.334	.458	-.332	.335	1.000									
NO_3^-	.827	.447	.521	-.373	.541	.943	1.000								
NH_4^+	.838	.423	.522	-.379	.462	.976	.987	1.000							
Cl^-	.855	.532	.618	-.477	.367	.745	.753	.804	1.000						
BC	.833	.851	.516	-.636	.465	.595	.691	.676	.732	1.000					
$C_2H_4O_2^+$	.761	.741	.431	-.536	.383	.560	.631	.629	.743	.864	1.000				
OOA	.834	.526	.510	-.419	.567	.901	.969	.957	.775	.746	.733	1.000			
COA	.499	.671	.223	-.398	.430	.272	.393	.351	.391	.638	.798	.502	1.000		
HOA	.590	.812	.286	-.567	.236	.302	.383	.376	.578	.812	.908	.493	.785	1.000	
BBOA	.606	.573	.407	-.439	.156	.352	.359	.383	.613	.728	.827	.433	.487	.816	1.000

Table S12 Correlation matrix of gaseous pollutants and particulate chemical compositions in submicron aerosols during the winter campaign.

	CO	NO_x	SO_2	CH_3CN	O_3	O_x	SO_4^{2-}	NO_3^-	NH_4^+	Cl^-	BC	$C_2H_4O_2^+$	LV-OOA	COA	SV-OOA	HOA	CCOA
CO	1.000																
NO_x	.933	1.000															
SO_2	.682	.702	1.000														
CH_3CN	.914	.895	.669	1.000													
O_3	-.763	-.757	-.701	-.712	1.000												
O_x	.692	.755	.561	.723	-.404	1.000											
SO_4^{2-}	.852	.826	.635	.852	-.635	.727	1.000										
NO_3^-	.813	.790	.627	.844	-.651	.804	.898	1.000									
NH_4^+	.854	.824	.652	.861	-.668	.777	.971	.971	1.000								
Cl^-	.790	.795	.572	.733	-.623	.555	.801	.666	.778	1.000							
BC	.922	.917	.646	.899	-.696	.749	.911	.850	.902	.874	1.000						
$C_2H_4O_2^+$	.833	.826	.555	.807	-.634	.644	.847	.774	.835	.889	.945	1.000					
MO-OOA	.562	.504	.493	.593	-.461	.702	.783	.872	.855	.463	.644	.603	1.000				
COA	.806	.879	.539	.808	-.655	.690	.765	.753	.778	.797	.859	.830	.480	1.000			
LO-OOA	.842	.880	.590	.844	-.556	.833	.887	.857	.877	.747	.902	.819	.627	.817	1.000		
HOA	.699	.658	.509	.666	-.587	.514	.797	.695	.781	.839	.839	.916	.666	.670	.636	1.000	
CCOA	.618	.561	.317	.520	-.515	.151	.432	.318	.387	.648	.635	.751	.086	.527	.408	.667	1.000

Table S13 Uncentered coefficients between mass spectra of COA factors during the seasonal campaigns in Beijing and the average from previous studies.

	Spring	**Summer**	**Autumn**	**Winter**	**Average**
Spring	1.000				
Summer	0.956	1.000			
Autumn	0.924	0.888	1.000		
Winter	0.893	0.977	0.835	1.000	
Average	0.977	0.990	0.910	0.954	1.000

S10 Assessment of secondary formation pathways

In this study, the LWC in aerosols was roughly estimated with the ISORROPIAII model. The input data were the four species (sulfate, nitrate, ammonium and chloride) measured by the AMS, the RH and temperature of ambient air. The reverse mode and the metastable state of aerosols were selected. According to the results, the ambient aerosols were generally in aqueous phase. The average values of aerosol LWC in four seasons were 17.3±28.5, 18.8±24.9, 12.8±27.3 and 25.2±32.8 $\mu g\ m^{-3}$, respectively. During the heavy-polluted episodes, the LWC was frequently higher than 100 $\mu g\ m^{-3}$.

It is well known that most of aerosol sulfate are formed from heterogeneous or aqueous-phase/cloud processes (Kulmala et al., 2016). On a global scale, about 80% of the sulfate formation occurs within clouds. Ambient aerosol populations often show two distinct submicron modes (<0.2 μm and 0.5–1 μm) where the larger (droplet) mode is formed from the smaller (condensation) mode through volume-phase reactions in clouds and wet aerosols (Ervens et al., 2011). Based on this assumption, Guo et al. (2010) found that the gas-to-particle condensation process was important for aerosol pollution in the summer of Beijing. In urban Beijing, the formation of sulfate was mainly attributed to in-cloud or aerosol droplet process (80%) and gas condensation process (14%).

Table S14 shows the correlation coefficients between OOA and some indicators (RH, LWC, O_3 and O_x). As shown in Table S14, secondary inorganics (sulfate and nitrate) correlated well with RH and/or LWC in four seasons, indicating that the aqueous-phase reactions in aerosols played an important role in secondary inorganic formation in Beijing. The contributions of photochemical processes to the formation of sulfate and nitrate in four seasons were likely less than those of aqueous-phase reactions according to the weaker correlations between secondary inorganics and odd oxygen (O_x=O_3+NO_2). Especially, in summer nitrate showed no correlation with O_x. As shown in Fig. S40, when RH was higher than 40% (or 30% in winter), aqueous-phase processed likely played a dominant role in secondary inorganic formation.

Table S14 Pearson correlation coefficients between secondary organic and inorganic species and some indicators (RH, LWC, O_3 and O_x). Coefficients greater than 0.5 are in bold. Correlation is significant at the 0.01 level (2-tailed) except for those marked by #.

		RH	LWC	O_3	O_x
Spring	OOA	**.661**	**.754**	-.199	.345
	SO_4^{2-}	**.764**	**.901**	-.207	.186
	NO_3^-	**.705**	**.827**	-.318	.254
Summer	MO-OOA	.176	**.751**	.131	.264
	LO-OOA	.005#	.469	.360	**.527**
	SO_4^{2-}	.114	**.686**	.262	.359
	NO_3^-	.335	**.873**	-.123	.000#
Autumn	OOA	.483	**.803**	-.433	**.571**
	SO_4^{2-}	**.552**	**.919**	-.340	.338
	NO_3^-	.489	**.854**	-.379	**.548**
Winter	MO-OOA	**.624**	**.647**	-.504	**.640**
	LO-OOA	**.692**	**.840**	-.534	**.726**
	SO_4^{2-}	**.801**	**.899**	-.613	**.597**
	NO_3^-	**.785**	**.819**	-.637	**.655**

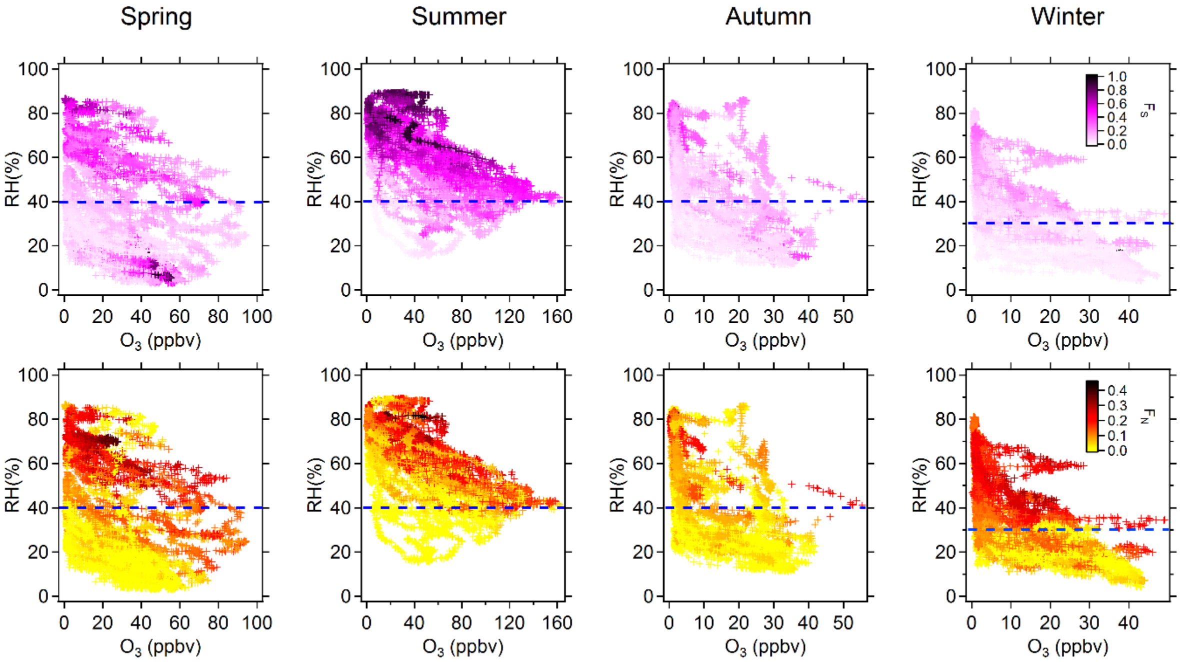

Figure S40. Influences of RH and O_3 concentrations on sulfate and nitrate formation.

Conversion ratios for sulfur and nitrogen (F_S and F_N) were calculated as follows:

$$F_S = \boldsymbol{n} - SO_4{}^{2-}/(\boldsymbol{n} - SO_4{}^{2-} + \boldsymbol{n} - SO_2) \qquad (3)$$

$$F_N = \boldsymbol{n} - NO_3{}^{-}/(\boldsymbol{n} - NO_3{}^{-} + \boldsymbol{n} - NO_2) \qquad (4)$$

where *n* means the amount of substance of the gaseous and particulate pollutants, mol m^{-3}.

The good correlation between F_N/F_S and RH/LWC also support that aqueous-phase reactions in aqueous aerosols and/or clouds could contribute to secondary inorganic formation remarkably in highly humid air.

Table S15 Pearson correlation coefficients between F_S and F_N with RH, LWC, O_3, O_x and NH_4^+.

	Spring		Summer		Autumn		Winter	
	F_S	F_N	F_S	F_N	F_S	F_N	F_S	F_N
RH	.339	**.722**	**.639**	.393	.432	**.574**	**.531**	**.744**
LWC	.475	**.816**	.464	**.816**	**.647**	**.874**	**.583**	**.676**
O_3	.024*	-.146	-.100	.024*	.035	-.321	-.268	-.518
O_x	-.166	.277	-.096	.052	-.122	.359	.342	.368
NH_4^+	.324	**.924**	.353	**.822**	.495	**.938**	**.598**	**.855**

Note: Coefficients greater than 0.5 are in bold. Correlation is significant at the 0.01 level (2-tailed) except for those marked with *.

Based on laboratory experiments and simulations, Ervens et al. (2011) suggest that SOA formed in cloud and aerosol water (aqSOA) might contribute almost as much mass as SOA formed in the gas phase to the SOA budget, with highest contributions from biogenic emissions of VOCs in the presence of anthropogenic pollutants (i.e., NO_x) at high RH and cloudiness. Xu et al. (2017) show that aqueous-phase processes have a dominant impact on the formation of MO-OOA, and the contribution of MO-OOA to OA increases substantially as a function of RH or liquid water content (LWC) in aerosols. In contrast, photochemical processing plays a major role in the formation of LO-OOA, as indicated by the strong correlations between LO-OOA and O_x during periods of photochemical production.

The good correlations between OOA and RH and/or LWC indicate that aqueous-phase reactions play a dominant role in OOA formation (Table S14). The slope of OOA against O_x steepened with the increase of RH and LWC (Figs. S41 and S42), also implying that the aqueous-phase oxidation was an important pathway of the OOA formation. The strong correlations between O_x and LO-OOA in summer, and between O_x and OOA in autumn and winter, suggesting photochemical processes also contributed substantially to OOA, especially LO-OOA, in these seasons.

It is difficult to give a quantitative result for the relative contribution of photochemical vs. aqueous-phase oxidation to the secondary formation based on field observation data only. Further studies including laboratory experiments, field observations and model simulations are needed to close the gaps in the current understanding of SOA formation pathways (Ervens et al., 2011).

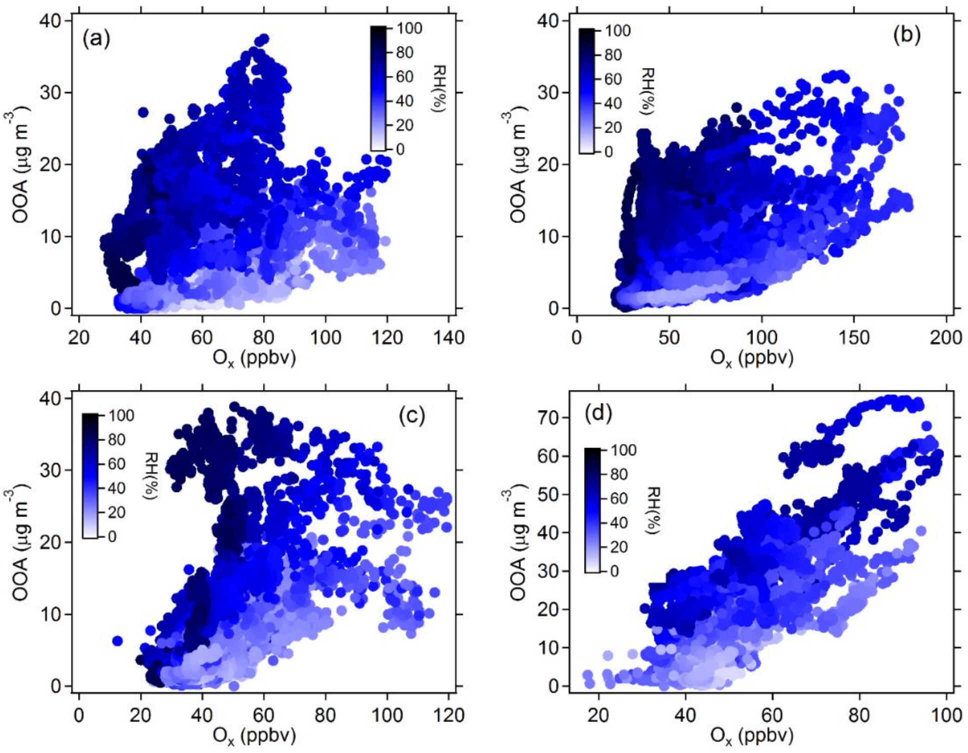

Figure S41. Scattering plots of OOA mass concentrations against O_x concentrations. (a) spring; (b) summer; (c) autumn and (d) winter. Data points are color coded by RH.

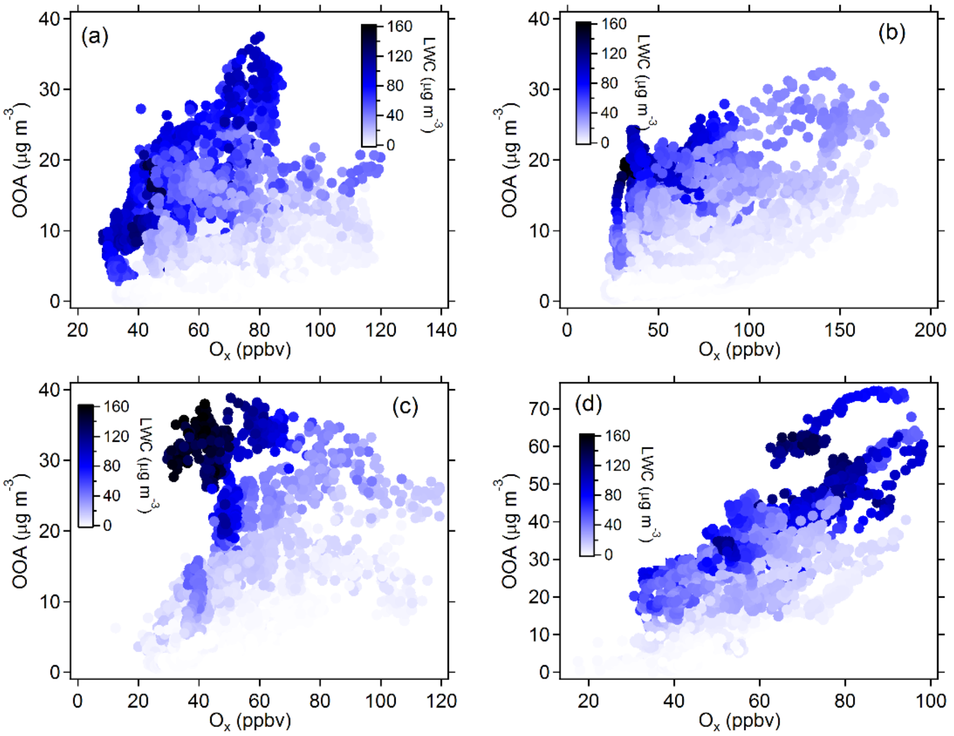

Figure S42. The same as above. Data points are color coded by estimated LWC in aerosols.

S11 Impacts of regional and long range transport on atmospheric aerosols

To give an insight into the impacts of regional/long-distance transport on atmospheric aerosols in Beijing, the backward trajectories of air parcels during the observation periods were calculated with the NOAA's HYSPLIT4 trajectory model (http://www.arl.noaa.gov/hysplit.html). A new 3-day backward trajectory was traced from the observation site at an altitude of 500 m above ground level every hour. Cluster analyses of backward trajectories were applied to reveal the major pathways during different campaigns (Fig. S43).

During the seasonal observations in Beijing, the pathways of dominant air masses are different. Both long-distance transported and regional/local air masses influenced Beijing. In summer, the transport distance of long-distance transported air masses was shorter than in other seasons. In general, with the decrease of transport distance, the concentration of PM_1 gradually increased. When Beijing was dominated by regional/local air masses, the fractions of secondary inorganic species (SNA) increased, while the contributions of carbonaceous components (OA+BC) decreased, which is consistent with the previous results in Beijing (Sun et al., 2010; Huang et al., 2010; Zhang et al., 2014). Higher concentrations of SNA and PM_1 under the control of regional/local air masses reflected the great contribution of secondary formation from the gaseous precursors (e.g., NO_x and SO_2) emitted by vehicles and coal combustion in urban areas.

During the observations in spring, summer and autumn, the contributions of OOA (MO-OOA+LO-OOA) increased when Beijing was dominated by regional or local air masses. In summer, the fractions of LO-OOA in OA were high (29–48%) regardless of the different trajectories, signifying that the secondary formation from photochemical oxidations probably made an important contribution to OA. During the winter observation, POA and OOA contributed equally to OA in most cases due to the long-lasting stable weather conditions, indicating that both primary pollutants and regional secondary formation made important contributions to OA. When Beijing was dominated by long-distance transported air masses from north polar regions in winter, OOA contributed more significantly to OA, implying that organic aerosols were fully aged during long-distance transport.

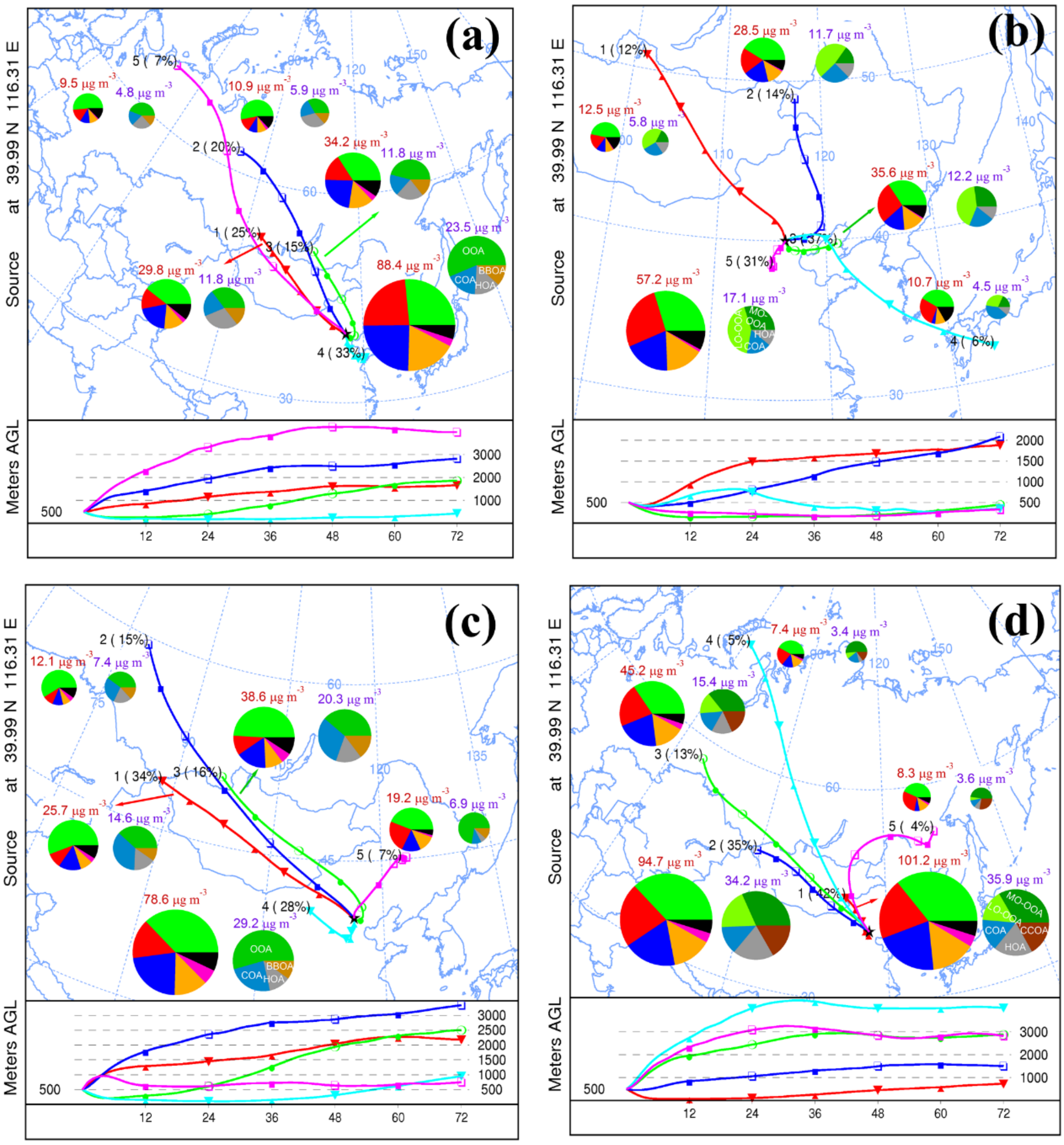

Figure S43. Back trajectories for each of the identified clusters and corresponding average main components of PM_1 and OA in PM_1 during the seasonal campaigns. (a) spring; (b)summer; (c) autumn and (d) winter. The filling color of main chemical species in PM_1 is the same with other figures.

References

Bae, M.-S., Demerjian, K. L., and Schwab, J. J.: Seasonal estimation of organic mass to organic carbon in $PM_{2.5}$ at rural and urban locations in New York state, Atmos. Environ., 40, 7467–7479, 2006.

Doshi, V., Vuthaluru, H. B., Korbee, R., and Kiel, J. H. A.: Development of a modeling approach to predict ash formation during co-firing of coal and biomass, Fuel Process Technol, 90, 1148-1156, doi: 10.1016/j.fuproc.2009.05.019, 2009.

Ervens, B., Turpin, B., and Weber, R.: Secondary organic aerosol formation in cloud droplets and aqueous particles (aqSOA): a review of laboratory, field and model studies, Atmos. Chem. Phys., 11, 11069-11102, 2011.

Grover, B. D., Eatough, N. L., Woolwine, W. R., Cannon, J. P., Eatough, D. J., and Long, R. W.: Semi-continuous mass closure of the major components of fine particulate matter in Riverside, CA, Atmos. Environ., 42, 250-260, 2008.

Guo, S., Hu, M., Wang, Z., Slanina, J., and Zhao, Y.: Size-resolved aerosol water-soluble ionic compositions in the summer of Beijing: implication of regional secondary formation, Atmos. Chem. Phys., 10, 947–959, doi:10.5194/acp-10-947-2010, 2010.

Hayes, P. L., Ortega, A. M., Cubison, M. J., Froyd, K. D., Zhao, Y., Cliff, S. S., Hu, W. W., Toohey, D. W., Flynn, J. H., Lefer, B. L., Grossberg, N., Alvarez, S., Rappenglück, B., Taylor, J. W., Allan, J. D., Holloway, J. S., Gilman, J. B., Kuster, W. C., de Gouw, J. A., Massoli, P., Zhang, X., Liu, J., Weber, R. J., Corrigan, A. L., Russell, L. M., Isaacman, G., Worton, D. R., Kreisberg, N. M., Goldstein, A. H., Thalman, R., Waxman, E. M., Volkamer, R., Lin, Y. H., Surratt, J. D., Kleindienst, T. E., Offenberg, J. H., Dusanter, S., Griffith, S., Stevens, P. S., Brioude, J., Angevine, W. M., and Jimenez, J. L.: Organic aerosol composition and sources in Pasadena, California, during the 2010 CalNex campaign, J. Geophys. Res. Atmos., 118, 9233-9257, 2013.

Hu, W. W., Hu, M., Yuan, B., Jimenez, J. L., Tang, Q., Peng, J. F., Hu, W., Shao, M., Wang, M., Zeng, L. M., Wu, Y. S., Gong, Z. H., Huang, X. F., and He, L. Y.: Insights on organic aerosol aging and the influence of coal combustion at a regional receptor site of central eastern China, Atmos. Chem. Phys., 13, 10095-10112, doi:10.5194/acp-13-10095-2013, 2013.

Hu, W. W., Hu, M., Hu, W., Jimenez, J. L., Yuan, B., Chen, W., Wang, M., Wu, Y., Chen, C., Wang, Z., Peng, J., Yang, K., Zeng, L., and Shao, M.: Chemical composition, sources and aging process of sub-micron aerosols in Beijing: contrast between summer and winter, J. Geophys. Res.-Atmos., 121, 1955–1977, doi:10.1002/2015JD024020, 2016.

Huang, X. F., He, L. Y., Hu, M., Canagaratna, M. R., Sun, Y., Zhang, Q., Zhu, T., Xue, L., Zeng, L. W., Liu, X. G., Zhang, Y. H., Jayne, J. T., Ng, N. L., and Worsnop, D. R.: Highly time-resolved chemical characterization of atmospheric submicron particles during 2008 Beijing Olympic Games using an Aerodyne High-Resolution Aerosol Mass Spectrometer, Atmos. Chem. Phys., 10, 8933-8945, 2010.

Jiang, Q., Sun, Y., Wang, Z., Yin, Y.: Real-time online measurements of the inorganic and organic composition of haze fine particles with an Aerosol Chemical Speciation Monitor (ACSM). Chin. Sci. Bull., 58, 3818-3828, 2013.

Kulmala, M., Petäjä, T., Kerminen, V.-M., Kujansuu, J., Ruuskanen, T., Ding, A., Nie, W., Hu, M., Wang, Z., Wu, Z., Wang, L., and Worsnop, D. R.: On secondary new particle formation in China, Front. Environ. Sci. Eng., 10, doi:10.1007/s11783-016-0850-1, 2016.

Lan, Z., Huang X., He, L., Hu, M., Xue, L., Sun, T., Hu, W., Lin, Y., Zhang Y. Comparison of measurement results of several online carbonaceous aerosol monitoring techniques. Acta Scientiarum Naturalium Universitatis Pekinensis, 47, 159-165, 2011.

Levin, E. J. T., McMeeking, G. R., Carrico, C. M., Mack, L. E., Kreidenweis, S. M., Wold, C. E., Moosmüller, H., Arnott, W. P., Hao, W. M., Collett, J. L., and Malm, W. C.: Biomass burning smoke aerosol properties measured during Fire Laboratory at Missoula Experiments (FLAME), J. Geophys. Res. Atmos., 115, doi: 10.1029/2009jd013601, 2010.

Lewis, K. A., Arnott, W. P., Moosmuller, H., Chakrabarty, R. K., Carrico, C. M., Kreidenweis, S. M., Day, D. E., Malm, W. C., Laskin, A., Jimenez, J. L., Ulbrich, I. M., Huffman, J. A., Onasch, T. B., Trimborn, A., Liu, L., and Mishchenko, M. I.: Reduction in biomass burning aerosol light absorption upon humidification: roles of inorganically-induced hygroscopicity, particle collapse, and photoacoustic heat and mass transfer, Atmos. Chem. Phys., 9, 8949-8966, 2009.

Li, J., Pósfai, M., Hobbs, P. V., and Buseck, P. R.: Individual aerosol particles from biomass burning in southern Africa: 2, Compositions and aging of inorganic particles, J. Geophys. Res. Atmos., 108, D13, 8484, 2003.

Liu, Q., Sun, Y., Hu, B., Liu, Z., Akio, S., and Wang, Y.: In situ measurement of PM1 organic aerosol in Beijing winter using a high-resolution aerosol mass spectrometer, Chin. Sci. Bull., 57, 819-826, 2011.

McNallan, M. J., Yurek, G. J., and Elliott, J. F.: The formation of inorganic particulates by homogeneous nucleation in gases produced by the combustion of coal, Combustion and Flame, 42, 45-60, doi:10.1016/0010-2180(81)90141-3, 1981.

Middlebrook, A. M., Bahreini, R., Jimenez, J. L., and Canagaratna, M. R.: Evaluation of Composition-Dependent Collection Efficiencies for the Aerodyne Aerosol Mass Spectrometer using Field Data, Aerosol Sci. Technol., 46, 258-271, doi:10.1080/02786826.2011.620041, 2012.

Sun, J., Zhang, Q., Canagaratna, M. R., Zhang, Y., Ng, N. L., Sun, Y., Jayne, J. T., Zhang, X., Zhang, X., and Worsnop, D. R.: Highly time- and size-resolved characterization of submicron aerosol particles in Beijing using an Aerodyne Aerosol Mass Spectrometer, Atmos. Environ., 44, 131-140, 2010.

Sun, Y., Wang, Z., Dong, H., Yang, T., Li, J., Pan, X., Chen, P., and Jayne, J. T.: Characterization of summer organic and inorganic aerosols in Beijing, China with an Aerosol Chemical Speciation Monitor, Atmos. Environ., 51, 250-259, 2012.

Sun, Y., Jiang, Q., Wang, Z., Fu, P., Li, J., Yang, T., and Yin, Y.: Investigation of the sources and evolution processes of severe haze pollution in Beijing in January 2013, J. Geophys. Res. Atmos., 119, 4380-4398, 2014.

Sun, Y. L., Wang, Z. F., Fu, P. Q., Yang, T., Jiang, Q., Dong, H. B., Li, J., and Jia, J. J.: Aerosol composition, sources and processes during wintertime in Beijing, China, Atmos. Chem. Phys., 13, 4577-4592, 2013.

Sun, Y. L., Zhang, Q., Schwab, J. J., Demerjian, K. L., Chen, W. N., Bae, M. S., Hung, H. M., Hogrefe, O., Frank, B., Rattigan, O. V., and Lin, Y. C.: Characterization of the sources and processes of organic and inorganic aerosols in New York city with a high-resolution time-of-flight aerosol mass apectrometer, Atmos. Chem. Phys., 11, 1581-1602, 10.5194/acp-11-1581-2011, 2011.

Xu, W., Han, T., Du, W., Wang, Q., Chen, C., Zhao, J., Zhang, Y., Li, J., Fu, P., Wang, Z., Worsnop, D. R., and Sun, Y.: Effects of Aqueous-Phase and Photochemical Processing on Secondary Organic Aerosol Formation and Evolution in Beijing, China, Environ. Sci. Technol., 51, 762-770, doi:10.1021/acs.est.6b04498, 2017.

Yokelson, R. J., Crounse, J. D., DeCarlo, P. F., Karl, T., Urbanski, S., Atlas, E., Campos, T., Shinozuka, Y., Kapustin, V., Clarke, A. D., Weinheimer, A., Knapp, D. J., Montzka, D. D., Holloway, J., Weibring, P., Flocke, F., Zheng, W., Toohey, D., Wennberg, P. O., Wiedinmyer, C., Mauldin, L., Fried, A., Richter, D., Walega, J., Jimenez, J. L., Adachi, K., Buseck, P. R., Hall, S. R., and Shetter, R.: Emissions from biomass burning in the Yucatan, Atmos. Chem. Phys., 9, 5785-5812, 2009.

Zhang, J. K., Sun, Y., Liu, Z. R., Ji, D. S., Hu, B., Liu, Q., and Wang, Y. S.: Characterization of submicron aerosols during a month of serious pollution in Beijing, 2013, Atmos. Chem. Phys., 14, 2887-2903, 2014.

Zhang, Q., Jimenez, J. L., Canagaratna, M. R., Allan, J. D., Coe, H., Ulbrich, I., Alfarra, M. R., Takami, A., Middlebrook, A. M., Sun, Y. L., Dzepina, K., Dunlea, E., Docherty, K., DeCarlo, P. F., Salcedo, D., Onasch, T., Jayne, J. T., Miyoshi, T., Shimono, A., Hatakeyama, S., Takegawa, N., Kondo, Y., Schneider, J., Drewnick, F., Borrmann, S., Weimer, S., Demerjian, K., Williams, P., Bower, K., Bahreini, R., Cottrell, L., Griffin, R. J., Rautiainen, J., Sun, J. Y., Zhang, Y. M., and Worsnop, D. R.: Ubiquity and dominance of oxygenated species in organic aerosols in anthropogenically-influenced Northern Hemisphere midlatitudes, Geophys. Res. Lett., 34, 2007.

Zhang, Y., Sun, J., Zhang, X., Shen, X., Wang, T., and Qin, M.: Seasonal characterization of components and size distributions for submicron aerosols in Beijing, Sci. China Earth Sci., 56, 890-900, 2013.

Bae, M.-S., Demerjian, K. L., and Schwab, J. J.: Seasonal estimation of organic mass to organic carbon in PM2.5 at rural and urban locations in New York state, Atmos. Environ., 40, 7467–7479, 2006.

Grover, B. D., Eatough, N. L., Woolwine, W. R., Cannon, J. P., Eatough, D. J., and Long, R. W.: Semi-continuous mass closure of the major components of fine particulate matter in Riverside, CA, Atmos. Environ., 42, 250-260, 2008.

Hu, W. W., Hu, M., Yuan, B., Jimenez, J. L., Tang, Q., Peng, J. F., Hu, W., Shao, M., Wang, M., Zeng, L. M., Wu, Y. S., Gong, Z. H., Huang, X. F., and He, L. Y.: Insights on organic aerosol aging and the influence of coal combustion at a regional receptor site of central eastern China, Atmos. Chem. Phys., 13, 10095-10112, 10.5194/acp-13-10095-2013, 2013.

Lan, Z., Huang X., He, L., Hu, M., Xue, L., Sun, T., Hu, W., Lin, Y., Zhang Y. Comparison of measurement results of several online carbonaceous aerosol monitoring techniques. Acta Scientiarum Naturalium Universitatis Pekinensis, 47, 159-165, 2011.

Sun, Y. L., Zhang, Q., Schwab, J. J., Demerjian, K. L., Chen, W. N., Bae, M. S., Hung, H. M., Hogrefe, O., Frank, B., Rattigan, O. V., and Lin, Y. C.: Characterization of the sources and processes of organic and inorganic aerosols in New York city with a high-resolution time-of-flight aerosol mass apectrometer, Atmos. Chem. Phys., 11, 1581-1602, 10.5194/acp-11-1581-2011, 2011.

Weimer, S., Drewnick, F., Hogrefe, O., Schwab, J. J., Rhoads, K., Orsini, D., Canagaratna, M., Worsnop, D. R., and Demerjian, K. L.: Size-selective nonrefractory ambient aerosol measurements during the Particulate Matter Technology Assessment and Characterization Study–New York 2004 Winter Intensive in New York City, J. Geophys. Res., 111, D18305, doi:10.1029/2006JD007215, 2006.